International Journal of Earth Sciences
https://doi.org/10.1007/s00531-021-02005-z

ORIGINAL PAPER

Tracing the SW border of the Svecofennian Domain in the Baltic Sea region: evidence from petrology and geochronology from a granodioritic migmatite

Evgenia Salin[1] · Jeremy Woodard[2] · Krister Sundblad[3]

Received: 16 September 2020 / Accepted: 28 January 2021

Abstract

Geological investigations of a part of the crystalline basement in the Baltic Sea have been performed on a drill core collected from the depth of 1092–1093 m beneath the Phanerozoic sedimentary cover offshore the Latvian/Lithuanian border. The sample was analyzed for geochemistry and dated with the SIMS U–Pb zircon method. Inherited zircon cores from this migmatized granodioritic orthogneiss have an age of 1854 ± 15 Ma. Its chemical composition and age are correlated with the oldest generation of granitoids of the Transscandinavian Igneous Belt (TIB), which occur along the southwestern margin of the Svecofennian Domain in the Fennoscandian Shield and beneath the Phanerozoic sedimentary cover on southern Gotland and in northwestern Lithuania. It is suggested that the southwestern border of the Svecofennian Domain is located at a short distance to the SW of the investigated drill site. The majority of the zircon population shows that migmatization occurred at 1812 ± 5 Ma, with possible evidence of disturbance during the Sveconorwegian orogeny.

Keywords Baltic Sea · Geochemistry · U–Pb · Zircon · TIB 0 · Svecofennian Domain

Introduction

The Precambrian basement in the Baltic Sea region is covered by km-thick successions of Phanerozoic sedimentary rocks, Quaternary sediments and overlying sea water. The relations between individual crustal segments in this region and the well-exposed adjacent Fennoscandian Shield have therefore historically been restricted to geophysical (gravity, magnetic and seismic) data, which have recorded a significant decrease in the crustal thickness towards the south in the central parts of the Baltic Sea (BABEL Working Group 1993; Lund et al. 2001).

✉ Evgenia Salin
evgenia.salin@utu.fi

1 Department of Geography and Geology, University of Turku, 20014 Turku, Finland

2 Geological Sciences, School of Agricultural, Earth, and Environmental Sciences, University of Kwa-Zulu Natal, Westville (Durban) X5 4001, South Africa

3 Institute of Earth Sciences, St. Petersburg State University, St. Petersburg 199034, Russian Federation

In a recent contribution, Salin et al. (2019) demonstrated that this geophysical feature is related to the border between two major crustal complexes in the Fennoscandian Shield; the Svecofennian Domain in the northeast and the Transscandinavian Igneous Belt in the southwest.

In this paper, the southwestern border of the Svecofennian Domain is further traced in the eastern parts of the Baltic Sea. Using petrographic, geochemical and geochronological evidence from migmatite drilled from beneath the east-central Baltic Sea, correlations are made with known magmatic and metamorphic events recorded in southeastern Sweden.

Geological background

Fennoscandian framework

The Fennoscandian Shield consists of a 2.9–2.6 Ga and older Archaean craton in the northeast, the ~1.92–1.87 Ga Svecofennian Domain intruded by the ~1.86–1.67 Ga Transscandinavian Igneous Belt (TIB) in the center and the 1.1–0.9 Ga Sveconorwegian orogen in the southwest (Fig. 1 inset; Gaál and Gorbatschev 1987; Gorbatschev and Bogdanova 1993; Bingen et al. 2005; Stephens and Weihed

Published online: 07 March 2021

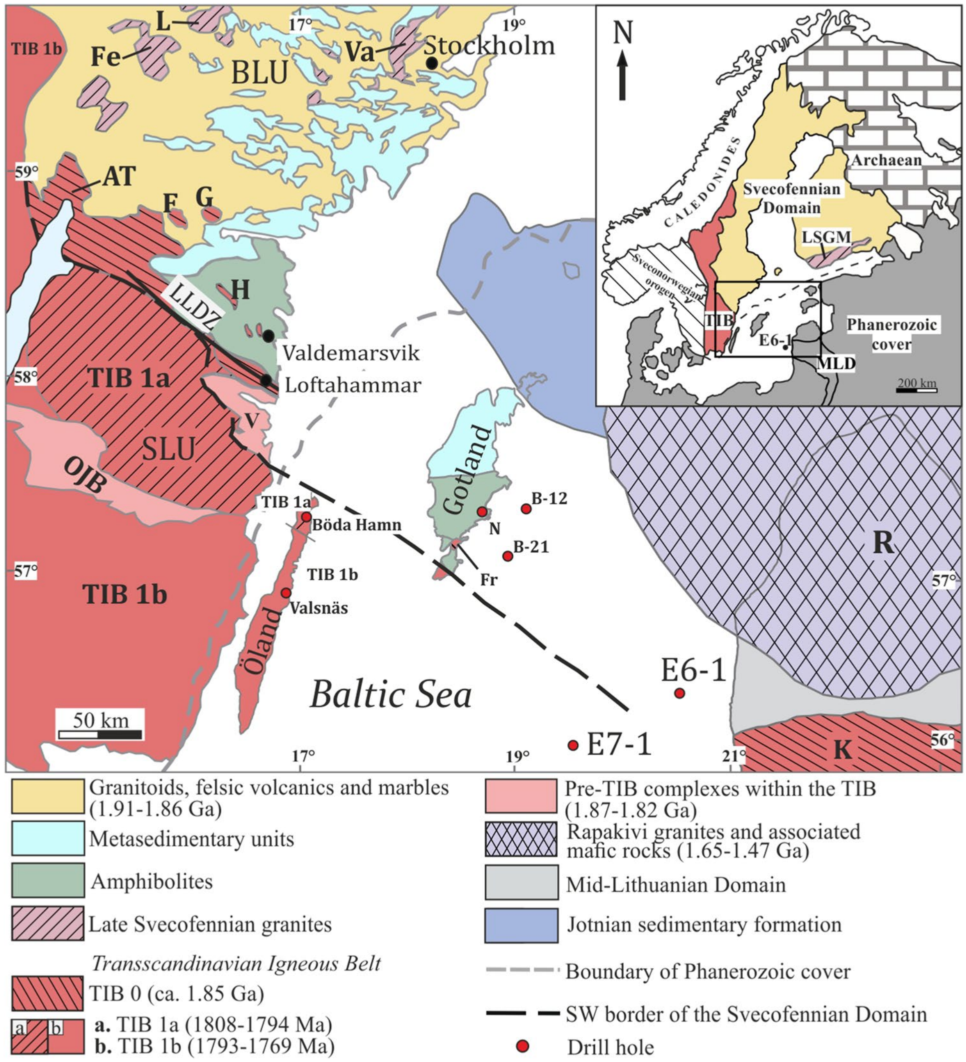

Fig. 1 Simplified geological map of the southern part of the Fennoscandian Shield including Precambrian units beneath the Phanerozoic cover in the Baltic Sea region. The map is modified after Koistinen et al. (2001) by adding information from Sundblad et al. (2003), Motuza and Motuza (2011) and Salin et al. (2019). *BLU* Bergslagen lithotectonic unit, *LLDZ* Loftahammar-Linköping deformation zone, *LSGM* Late Svecofennian granite-migmatite zone, *OJB* Oskarshamn-Jönköping belt, *R* Riga batholith, *SLU* Småland lithotectonic unit, *TIB* Transscandinavian Igneous Belt, *V* Västervik quartzites, *WLG* West Lithuanian Granulite domain. The TIB 0 granites: *F* Finspång, *G* Graversfors, *H* Hälla, *AT* Askersund-Tiveden area, *K* Kuršiai. Late Svecofennian granites: *Fe* Fellingsbro, *L* Lisjö, *Va* Vallentuna. The location of E6-1 and other drill sites of interest for this study are marked with red dots. Drill sites: *Fr* Frigsarve, *N* När

2020). The geological evolution in the earliest Proterozoic (2.5–2.0 Ga) was manifested by protracted extension and rifting of the craton and formation of oceanic basins along its western and southern margins. The Svecofennian crust was mainly formed from 1.92 to 1.87 Ga, which represents continued marine conditions to the west of the craton and associated formation of juvenile crust associated with several magmatic arcs, which eventually amalgamated with the Archaean continent (Korja et al. 2006; Stephens 2020). Supracrustal rocks of the domain include metavolcanic and intercalated metasedimentary successions formed between 1.96 and 1.84 Ga (e.g. Skiöld 1988; Welin 1992).

Svecofennian magmatic rocks have traditionally been divided into early and late orogenic (Gaál and Gorbatschev 1987). The intrusion of extensive early Svecofennian granitoids commenced almost simultaneously with calc-alkaline volcanism (Allen et al. 1996; Stephens et al. 2009; Kampmann et al. 2016). The oldest granitoid plutons consist of a differentiated suite of calcic and calc-alkaline, I-type rocks that range in composition from gabbroic to granodioritic and granitic. They form large plutonic complexes in central Finland and Sweden. Although the early Svecofennian plutonism is mostly restricted to 1.92–1.87 Ga, intrusive activity lasted locally until 1.85 Ga (Vaasjoki and Sakko 1988; Väisänen et al. 2002). A first stage of metamorphism affecting the Svecofennian crust was recorded at 1.87 Ga by Andersson et al. (2006) in the Bergslagen area, leading to the creation of a Fennoscandian proto-continent. Subsequent crustal reworking, resulting in the final cratonization of the Svecofennian units, caused the formation of migmatites, anatectic partial melts and the emplacement of late Svecofennian I- and S-type granites at 1.83–1.80 Ga (e.g. Vaasjoki and Sakko 1988; Lindh 2014).

The emplacement ages for the late Svecofennian granites span from 1.85 to 1.79 Ga in southern Finland, Late Svecofennian granite-migmatite zone (LSGM, Fig. 1 inset; e.g. Kurhila et al. 2011; Skyttä and Mänttäri 2008). In Bergslagen, the late Svecofennian granites have ages ranging from 1.84 to 1.75 Ga (Öhlander and Zuber 1988; Stephens and Andersson 2015; Johansson and Stephens 2017). The granites occur as two principal types: large homogeneous massifs of coarse-grained porphyritic K-feldspar granites (e.g. Fellingsbro, Lisjö) or smaller intrusions of heterogeneous granites associated with migmatites (e.g. Vallentuna granite complex).

Continued extension along the western border of the Svecofennian Domain resulted in the emplacement of the 1.85–1.65 Ga Transscandinavian Igneous Belt (TIB; Gaál and Gorbatschev 1987). The southern part of the Svecofennian Domain was intruded by anorogenic rapakivi granites at 1.64–1.47 Ga (e.g. Ahl et al. 1996; Rämö and Haapala 2005). The westernmost component of the Fennoscandian Shield was reworked and polyphaser-deformed during the Sveconorwegian orogeny at 1.1–0.9 Ga (Bingen et al. 2005).

Bergslagen lithotectonic unit

The southwestern part of the Svecofennian Domain is composed of two major lithotectonic units: Bergslagen and Småland (Fig. 1; Stephens 2020). The Småland unit is dominated by post-Svecofennian units, mainly TIB (Jarl and Johansson 1988; Mansfeld 1991; Kleinhanns et al. 2015), distinguished based on the mode of deformation and metamorphic conditions (Stephens et al. 1997; Korja and Heikkinen 2005). The southern border of the Bergslagen lithotectonic unit runs along the Loftahammar-Linköping deformation zone (LLDZ), which separates it from the Småland lithotectonic unit (Stephens et al. 1997; Beunk and Page 2001; Wik et al. 2005). The LLDZ is a shear belt of several kilometers width which is composed of strongly banded orthogneisses. The age dating indicates that the rocks have undergone ductile strain under amphibolite facies conditions in the time interval 1.86–1.85 Ga (Stephens and Andersson 2015), but later was reactivated in colder, brittle regimes (Stephens and Jansson 2020). The LLDZ extends from southeastern Sweden through Gotland towards the Latvian coast (Korja and Heikkinen 2005).

The Bergslagen lithotectonic unit is dominated by metamorphosed 1.91–1.86 Ga early Svecofennian granitoids, diorite and gabbro showing a calc-alkaline affinity (Stephens et al. 2009). The southernmost position for such a rock unit is 17 km south of Valdemarsvik (Fig. 1), where Stephens and Andersson (2015) documented a 1.88 Ga age for an early Svecofennian granodioritic orthogneiss. Felsic metavolcanic rocks, with subordinate carbonate and siliciclastic metasedimentary rocks of similar or older ages, are also prominent in most parts of the Bergslagen region. However, amphibolite is the dominating supracrustal rock in the southernmost segment (Valdemarsvik area). Subsequent igneous activity related to mafic underplating and anatexis took place at 1.87–1.85 Ga and 1.84–1.81 Ga and partly overlaps in space and time with the emplacement of the TIB felsic intrusive rocks (Stephens and Andersson 2015; Johansson and Stephens 2017). Late Svecofennian migmatites and pegmatites are mostly observed in the southeastern and northern parts of the Bergslagen area (Andersson 1997; Hermansson et al. 2007; Stephens et al. 2009).

The southern parts of the Bergslagen lithotectonic unit were affected by unevenly distributed ductile foliation (D1) developed prior to static recrystallization of the rocks. Later folding (D2) of the boundaries between the rock units and the tectonic foliation occurred at different scales (Hermansson et al. 2007; Stephens et al. 2009). Metamorphic temperatures correspond to amphibolite or granulite facies conditions (Stephens et al. 2009; Stephens and Andersson 2015). The southern parts of the Bergslagen lithotectonic unit were also subject to high-grade metamorphism involving partial melting with development of migmatites. Mineral parageneses with andalusite (or sillimanite), cordierite and garnet in aluminous rocks, as well as geobarometric and geothermometric data indicate metamorphism under low-P conditions at 4–6 kbar (Stephens et al. 2009; Johansson and Stephens 2017). Stephens and Andersson (2015) and Andersson et al. (2006) showed that two metamorphic events, associated with anatexis under low-pressure conditions in the central and southern parts of the Bergslagen lithotectonic unit, took place at ≤ 1.87 Ga (M1) and 1.84–1.81 Ga (M2) intimately associated with the D1 and D2 deformation events (accordingly). The age of 1854 Ga was recorded for the Askersund granites in the Tiveden area by Wikström (1996), whereas Andersson (1997) recorded an 1818 Ma age of contact metamorphism in the same area.

Småland lithotectonic unit

The Småland lithotectonic unit (Fig. 1) mainly consists of three generations of felsic intrusive rocks belonging to the Transscandinavian Igneous Belt: TIB 0 (1855–1845 Ma), TIB 1a (1808–1794 Ma) and TIB 1b (1793–1769 Ma); (Larson and Berglund 1992; Ahl et al. 2001; Salin et al. 2019). The oldest generation, TIB 0, occurs mainly in the Bergslagen lithotectonic unit (Askersund-Tiveden areas, as well as the Finspång, Graversfors and Hälla intrusions), and compositionally has been assigned by Stephens et al. (2009) to the 1.87–1.84 Ga intrusive suite of the Bergslagen lithotectonic unit. Nevertheless, the TIB 0 granitoids are also observed in the northeastern part of the Småland lithotectonic unit (Loftahammar area), which is suggested to be reminiscent of the Bergslagen lithotectonic unit inside the Småland lithotectonic unit representing a tectonic link between Bergslagen and Småland units (Wahlgren and Stephens 2020).

The TIB 0 granitoids are quartz monzonites and quartz syenites with alkali-calcic metaluminous to peraluminous geochemical signatures (Andersson 1997; Ahl et al. 2001).

All other parts of the Småland lithotectonic unit are dominated by I-type quartz monzonites to granites constituting homogeneous TIB 1a and heterogeneous TIB 1b granitoid generations. In the central part of the unit, the E-W trending Oskarshamn-Jönköping Belt (OJB) was formed between 1.83 and 1.82 Ga (Mansfeld 1996; Åhäll et al. 2002) and separates the TIB 1a from the TIB 1b granitoids. The OJB is dominated by a continuous belt of calc-alkaline tonalites to granodiorites emplaced between 1.83 (Mansfeld 1996; Åhäll et al. 2002) and 1.82 Ga (Wik et al. 2003). The supracrustal rocks of the OJB include felsic and mafic volcanic rocks of the Fröderyd Group (Sundblad et al. 1997), volcanic and volcano-sedimentary formations in the Nömmen area and the Vetlanda metasedimentary formation (Röshoff 1975). The 1.85 Ga age was recorded by Salin et al. (2020) for a metamorphosed rhyolite in the Fröderyd Group indicating the oldest crustal component southwest of the Svecofennian Domain.

Southwestern limit of the Svecofennian Domain

The Västervik metasedimentary succession has a key position in the understanding of the evolution along the southwestern margin of the Svecofennian Domain. It is a km-thick continental margin sequence of fluvial, tidal and turbiditic deposits with 3.64–1.87 Ga detrital components (Sultan et al. 2005; Sultan and Plink-Björklund 2006). The presence of metabasaltic intercalations or dykes (Kresten 1972) indicates that the sedimentation was associated with some kind of rifting. The U–Pb ages of the two youngest detrital grains (1872 ± 24 Ga and 1870 ± 12 Ma) demonstrate that deposition in this basin cannot have started until shortly after the first metamorphic event (1.87 Ga) of the Svecofennian crust recorded by Andersson et al. (2006) in the adjacent Bergslagen area. The sedimentation in the Västervik basin must, however, have been completed already before 1859 ± 9 Ma, when the TIB 0 granitoids of Loftahammar intruded into the Västervik succession (Bergström et al. 2002) and sealed it to the Svecofennian granitoids and amphibolites in the Valdemarsvik area and thus the Fennoscandian proto-continent. For this reason, it is considered relevant to include the Västervik succession in the concept "Svecofennian Domain".

Baltic Sea region

The Precambrian crystalline bedrock continues beneath the Baltic Sea where it is covered by up to 2300 m thick sequences of Phanerozoic sedimentary rocks of the East European Platform (Fig. 1; Bogdanova et al. 2015; Salin et al. 2019). The Precambrian bedrock beneath Gotland and adjacent offshore region has been studied through drillings (approximately 35 percussion drillings and drill cores; Sundblad et al. 2003; Salin et al. 2019) and geophysical investigations (EUROBRIDGE seismic working group 1999). Amphibolite is the dominant Svecofennian supracrustal rock unit beneath the sedimentary cover on southern Gotland. On the southernmost tip of Gotland, it is intruded by the TIB 1a unit (Sundblad et al. 2003). The amphibolite is also intruded by 1.88 Ga orthogneisses at När (Sundblad et al. 2003) and TIB 0 granitoids at Frigsarve (Salin et al. 2019), which correlates well with the Hälla-Valdemarsvik and Loftahammar regions.

Furthermore, early Svecofennian Pb-Pb signatures in igneous K-feldspar grains were recorded by Salin (2014) in two offshore drill cores, B-12 and B-21, east of southern Gotland (Fig. 1). The southwestern border of the Svecofennian Domain has been drawn in Fig. 1 from the southwestern side of the Västervik quartzites in the Fennoscandian Shield to the southwestern limit of the amphibolites on southernmost Gotland.

Western Latvia and Lithuania

The Precambrian rocks in western Latvia and Lithuania are also concealed by a thick cover of Phanerozoic sedimentary rocks (Fig. 1 inset), but have been studied through numerous drill cores (e.g. Skridlaite and Motuza 2001) and geophysical investigations (EUROBRIDGE seismic working group 1999; Bogdanova et al. 2006).

The Mid-Lithuanian Domain (MLD) occupies the northwestern and northern parts of Lithuania and continues farther north in the Precambrian basement of western Latvia. The MLD is a composite domain characterized by charnockitic rocks (sensu lato) and mafic granulites in the north and northwest (Kuršiai pluton) and migmatites and granites in the northeast. Supracrustal rocks of the MLD include metamorphosed felsic volcanic and sedimentary sequences. The tectonic setting was transitional from a volcanic island arc in the south to active continental margin in the north (Motuza et al. 2008; Bogdanova et al. 2015).

Based on U–Pb and Sm–Nd isotopic characteristics, Mansfeld (2001) implied that the Precambrian basement beneath the Phanerozoic cover in Latvia and Lithuania was formed between 1.9 and 1.82 Ga, which together with lithological similarities suggests a continuation of the Svecofennian Precambrian rocks in this area. Formation of charnockites and garnet-cordierite-bearing granites (Kuršiai pluton) occurred during the time interval of 1850–1815 Ma (Claesson et al. 2001; Motuza et al. 2008). The final stage of magmatism coincides with the granulite peak metamorphism recorded in the metasedimentary rocks at 1.81–1.79 Ga (Claesson et al. 2001; Skridlaite et al. 2014). This metamorphic age is not documented in the MLD charnockites, except for some alteration in the magmatic zircon at 1.79–1.74 Ga (Skridlaite et al. 2014).

The northernmost extent of the MLD is defined by the intrusion of the ~ 1.58 Ga Riga pluton, a rapakivi-anorthosite suite (Kirs et al. 2004). The western border of the MLD is not well defined, however, based on geochemical and geochronological data, Motuza and Motuza (2011) correlated the 1.85 Ga Kuršiai plutonic suite with the TIB 0 granitoids in southeastern Sweden.

Materials and methods

Materials

The Precambrian basement in the study area is covered by a km-thick sequence of Phanerozoic sedimentary rocks and ~ 100 m of seawater, and all access to study material is restricted to drill core material. The sample for this study comes from the drill core E6-1 (Figs. 1, 2), courtesy of the Geological Survey of Latvia. This drilling was conducted as a part of a program with the main purpose to document stratigraphy of the Palaeozoic sedimentary sequences. All available geophysical, geological and borehole data starting from 1980 had been used to produce geological maps of the Baltic Sea and compiled in a map description by Grigelis (1991). According to Grigelis (1991), the Phanerozoic cover in the E6-1 drill core is composed of Cambrian-Devonian sedimentary rocks (e.g. dolomites, sandstones and claystone); the Precambrian basement is encountered at the depth of 1045 m (Fig. 2a). The crystalline basement is composed of Mesoproterozoic sedimentary and volcanic rocks (1045–1056 m) and underlying Palaeoproterozoic migmatites (1056–1095 m). The migmatite is cut by a 3 cm wide lamprophyre dyke at 1095 m. Our sample from the E6-1 drill core was collected from the depth interval of 1092.0–1093.0 m and is composed of a migmatitic orthogneiss containing dark grey melanocratic and bright pink leucocratic domains (Fig. 2b, c).

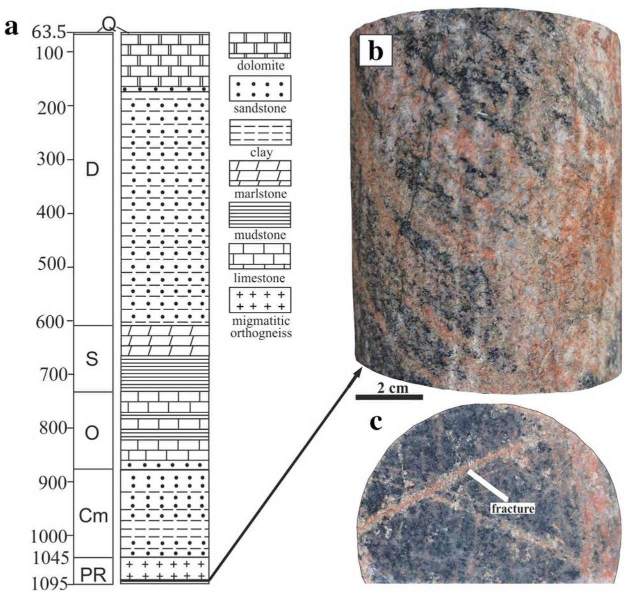

Fig. 2 **a** Generalized geological section of the E6-1 drill hole (after Grigelis 1991). The sampling depth (1092.0–1093.0 m) is marked with a thick line; **b** The sample from the E6-1 drill hole investigated in this study. Migmatitic orthogneiss with grey granodioritic palaeosome and red granitic leucosome domains displaying gneissose texture; **c** Fracture filled with adularia that is reddish-brown colored due to micrograins of hematite. Some calcite is also present in the fractures

Analytical methods

Melanocratic and leucocratic layers are rather thin and the contact between them is gradational (Fig. 2). Separate rock pieces of each layer were cut from the core sample using a rock saw, discarding diffuse contact areas and carbonate-quartz veins. These were analyzed for geochemistry at either CAF, Stellenbosch University, South Africa, or Actlabs, Ontario, Canada (Table 1). Methods at Stellenbosch employ XRF and LA-ICP-MS from fusion glass, while Actlabs uses fusion inductively coupled plasma spectrometry (FUS-ICP) and fusion mass spectrometry (FUS-MS) methods. The F content was determined by fusion ion-selective electrode (FUS-ISE). No significant deviation in results is observed between the two laboratories.

For the zircon study, a composite sample of both melanocratic and leucocratic components was used. As a result of the thin layered structure and diffuse contact between the components, it was assumed that the similarity in thermochemical history between the two domains was not sufficiently distinct to warrant two separations. Furthermore, combining the components ensured a significant population of zircons from the limited material available. Zircon separates from the sample were obtained using a conventional heavy liquid method. Magnetic minerals were removed using Frantz magnetic separator. The zircon grains were handpicked from a heavy fraction under a binocular microscope and cast together with the 1065 Ma Geostandard reference zircon 91,500 in an epoxy mount (Wiedenbeck et al. 2004) for SIMS analyses. After hardening, mounts were polished to approximately half of zircon thickness to reach the core of a grain. Back-scattered electron (BSE) images were prepared to study growth features and to target the spot analysis sites using JEOL TM JSM-7100F Field Emission Scanning Electron Microscope at the Geological Survey of Finland in Espoo.

The U-(Th)-Pb analysis of the E6-1 sample was conducted using a large geometry Cameca IMS1280 Secondary Ion Mass Spectrometer (SIMS) at the Swedish Museum of Natural History in Stockholm (Nordsim facility). The SIMS instrument setup parameters generally followed those described in

Table 1 Chemical composition of the E6-1 migmatitic orthogneiss

Sample	E6-1						Detection limit
	leucosome			palaeosome			
	A[a]	B[b]	C[b]	A[a]	B[b]	C[b]	
Major elements (wt%)							
SiO_2	66.43	67.72	67.95	63.78	65.46	63.98	0.01
Al_2O_3	13.5	13.87	13.86	14.59	14.81	14.81	0.01
Fe_2O_3t	2.93	3.39	3.39	6.02	5.91	6.61	0.01
MnO	0.05	0.04	0.04	0.06	0.06	0.07	0.001
MgO	0.7	0.69	0.7	1.18	1.26	1.41	0.01
CaO	1.65	1.56	1.66	3.78	3.44	3.49	0.01
Na_2O	2.64	2.85	3	2.89	2.99	2.9	0.01
K_2O	7.35	6.29	6.19	3.46	3.42	3.48	0.01
TiO_2	0.36	0.44	0.41	0.89	0.89	0.88	0.001
P_2O_5	0.14	0.17	0.16	0.24	0.26	0.26	0.01
F	0.13			0.07			0.01
LOI	3.24	3.47	3.34	1.92	2.18	2.38	0.01
Total	99	100.49	100.7	98.82	100.69	100.25	
Trace elements (ppm)							
Sc	6	11	11	17	18	23	1
Be	2			4			1
V	31	42	42	74	81	81	5
Ba	876	865	994	470	437	455	2
Sr	209	167	184	117	113	111	2
Y	13	14	14	22	20	23	1
Zr	105	185	102	245	295	290	2
Cr	20	14	11	20	22	24	20
Co	4	6	5	11	12	13	1
Ni	20	11	9	20	18	18	20
Cu	10	13	13	20	42	29	10
Zn	30	49	49	70	89	98	30
Ga	17			19			1
Ge	1			1			1
As	5			5			5
Rb	224	191	177	165	150	153	2

Sample	E6-1						Detection limit
	leucosome			palaeosome			
	A	B	C	A	B	C	
Nb	39	36.7	44.5	9	17.7	15.7	1
Mo	2	0.8	0.9	2	1.3	2.4	2
Ag	0.5			0.6			0.5
In	0.2			0.2			0.2
Sn	3			1			1
Sb	0.5			0.5			0.5
Cs	1.4	1.4	1.1	4.7	4	4.1	0.5
Hf	2.3	4.8	2.8	5.6	7.7	7.6	0.2
Ta	0.7	0.7	0.7	0.6	0.7	0.7	0.1
W	3			1			1
Tl	0.8			0.6			0.1
Pb	18	19.6	19.2	14	15.8	18.5	5
Bi	0.4			0.4			0.4
Th	13.3	18	19.4	8.7	8.5	10.3	0.1
U	1.1	1	1.2		0.8	0.8	0.9
Rare earth elements (ppm)							
La	57.3	67.8	78.8	50.8	51.3	52.9	0.1
Ce	113	136.6	161	103	105.2	109	0.1
Pr	11.7	14.7	17.1	11.9	12	12.6	0.05
Nd	40.4	54.9	62.9	45.9	48.6	51.6	0.1
Sm	6.1	8.7	9.1	9.1	9.3	9.6	0.1
Eu	1.9	2.06	2.07	1.65	1.67	1.66	0.05
Gd	3.9	6.1	5.5	7.6	7.6	7.9	0.1
Tb	0.5	0.7	0.6	1	1	1	0.1
Dy	2.7	3.4	3	5	4.8	5.6	0.1
Ho	0.5	0.5	0.5	0.8	0.8	0.9	0.1
Er	1.3	1.4	1.5	1.9	1.9	2.3	0.1
Tm	0.17	0.18	0.19	0.22	0.22	0.25	0.05
Yb	1	1.2	1.3	1.3	1.3	1.5	0.1
Lu	0.15	0.16	0.19	0.18	0.18	0.22	0.01
$(La/Yb)_{PM}$	39	38.5	40.9	26.6	26.9	24.1	

[a]Analyses conducted at Actlabs, Canada

[b]Analyses conducted at CAF, Stellenbosch University, South Africa

Whitehouse et al. (1999) and Whitehouse and Kamber (2005). A 23 kV incident energy (− 13 kV primary, + 10 kV secondary) O^{2-} primary beam was used in aperture illumination (Köhler) mode, resulting in a ~ 15 µm spot. Age calculations were performed using version 4.15 of the Isoplot software (Ludwig 2003).

Results

Petrography and nomenclature remarks

In hand specimen, the migmatite is dominated by a medium-grained melanocratic domains with gneissic structure. This irregularly alternates with a coarse-grained homogeneous granitic domains creating a gneissose banding (Fig. 2b). Melanocratic and leucocratic domains have both diffuse and sharp contacts. The rock is cut by narrow veins filled with carbonate and quartz as well as fractures filled with hematite and adularia (Fig. 2c).

Quartz, plagioclase, and biotite form up to 90% of the melanocratic domains (Fig. 3a). Rare K-feldspar and titanite grains are also observed. The titanite grains replace biotite and the plagioclase grains exhibit myrmekitic and antiperthitic textures (Fig. 3a). The plagioclase grains are sometimes replaced by clinozoisite, sericite and epidote. Small cracks in quartz and altered plagioclase crystals are filled with sericite/muscovite (Fig. 3a). At least two quartz generations are present: larger (up to 0.01 mm) crystals as well as recrystallized finer-grained (0.001–0.003 mm) metasomatic quartz replacing plagioclase and biotite. Some clusters of quartz grains are characterized by triple junctions (Fig. 3b), indicating grain boundary migration. The biotite and plagioclase grains are bent and kinked (Fig. 3c), which together with the observation of deformation twins of plagioclase (Fig. 3c) and formation of small quartz crystals, indicate deformation in a solid state. Accessory minerals are apatite,

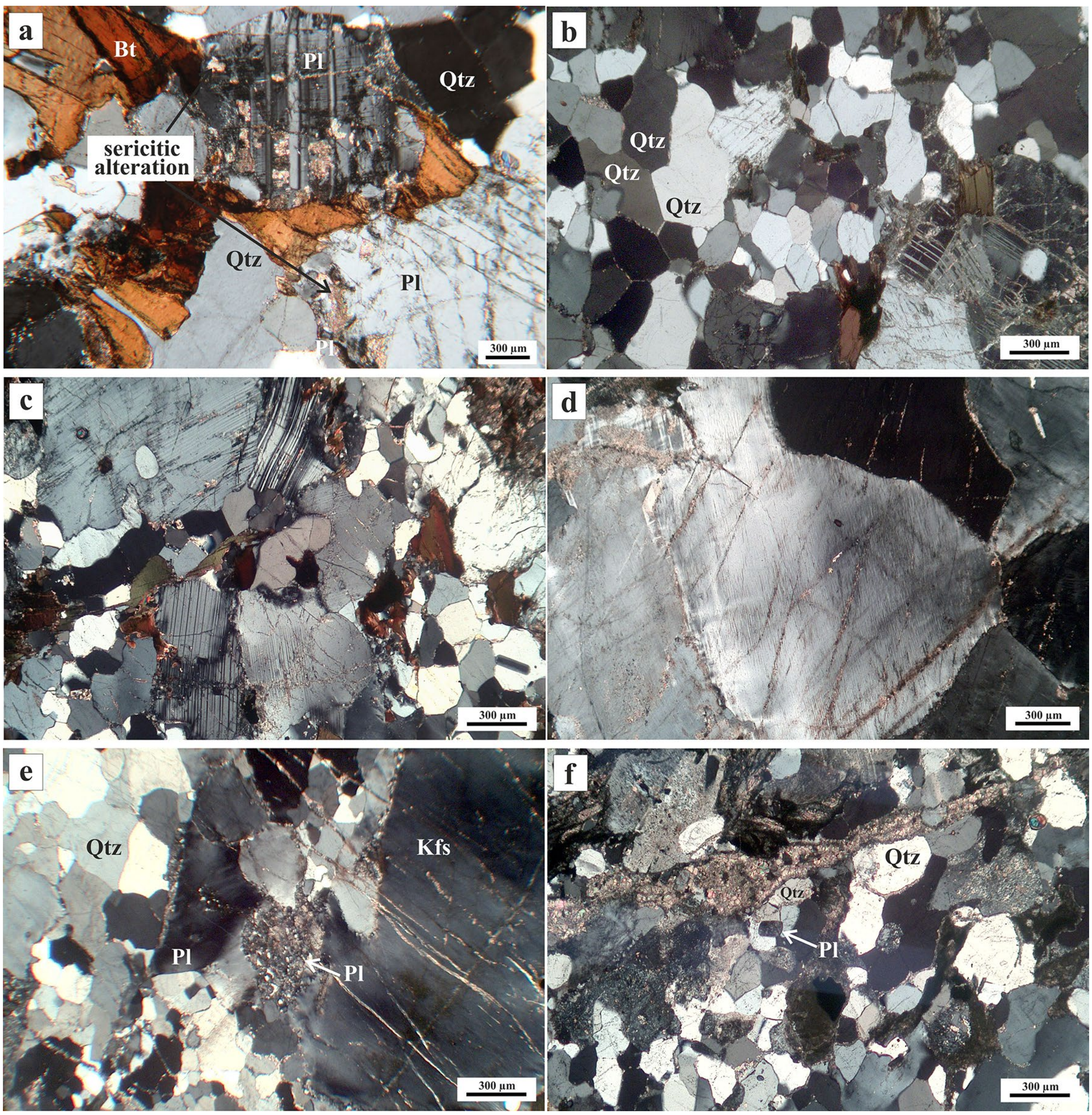

Fig. 3 The sample from the E6-1 drill hole. **a** Plagioclase grains showing antiperthite unmixing and sericitic alteration in the palaeosome; **b** Clusters of quartz grains characterized by triple junctions in the palaeosome; **c** Bent plagioclase grains and deformation twins in plagioclase in the palaeosome; **d** Perthitic K-feldspar grain slightly altered by sericite in the leucosome; **e** Myrmekites in altered plagioclase grain in the leucosome; **f** Altered euhedral plagioclase grain surrounded by quartz in the leucosome

epidote, zircon, ilmenite and magnetite. Only one garnet inclusion (26 µm in diameter) was observed in zircon by EDS, Energy Dispersive X-Ray Spectroscopy.

The leucocratic domains are dominated by medium- to coarse-grained quartz and feldspars (Fig. 3b). In hand specimen, the rock is homogeneous and massive with feldspar grains up to 1 cm in diameter. Plagioclase and K-feldspar are in equal proportions. Minor biotite is present. Alteration types in the leucocratic domains are the same as in the melanocratic domains. Plagioclase grains are partly sericitized and contain myrmekites (Fig. 3e), while K-feldspar (oligoclase) is mostly devoid of alteration and exhibits perthitic texture (Fig. 3d). Some plagioclase grains that occur within quartz are euhedral, although affected by sericitic alteration (Fig. 3f). Accessory minerals include rutile partly replaced by titanite, apatite, zircon, ilmenite and magnetite.

In terms of Sawyer (2008), neosome is a part of a migmatite newly formed by partial melting, whereas palaeosome is a non-neosome part that was not affected by partial melting. A leucosome is defined as a light-colored part of the neosome, dominantly composed of feldspar and quartz (ibid). A melanosome is a darker-colored part of the neosome, dominantly composed of biotite, garnet, cordierite, orthopyroxene, clinopyroxene and hornblende. If an anatectic melt has migrated from the place where it was formed, then it is an in-source leucosome, while an anatectic melt remained at site where the melt was formed is an in situ leucosome (Sawyer 2008). Although it is difficult to define what has been melted and what has not, a palaeosome coexisting with the neosome cannot be unaffected by partial melting, and the palaeosome can be distinguished from the neosome. Palaeosome is a rock, which preserved its structures (such as foliations, folds, layering), and the microstructures are either unchanged or slightly coarsened (Sawyer 2008). Melanocratic material in the E6-1 drill core preserved gneissose structure, and it has much smaller grain size compared to massive and coarser grained leucocratic parts. Some of the plagioclase crystals that occur within quartz are euhedral, which is interpreted to indicate crystallization from a melt. Thus, melanocratic material belongs to a palaeosome, while leucocratic material belongs to a leucosome. Although the obtained section of the E6-1 drill core did not have a definitive melanosome, we cannot exclude presence of one in the migmatite. However, lack of melanosome and some sharp contacts between melanocratic and leucocratic domains may also suggest that the leucosome was formed in an open system (in-source leucosome) implying that it has migrated within the margins of its source layer. The term "melanosome" will be used in the discussion.

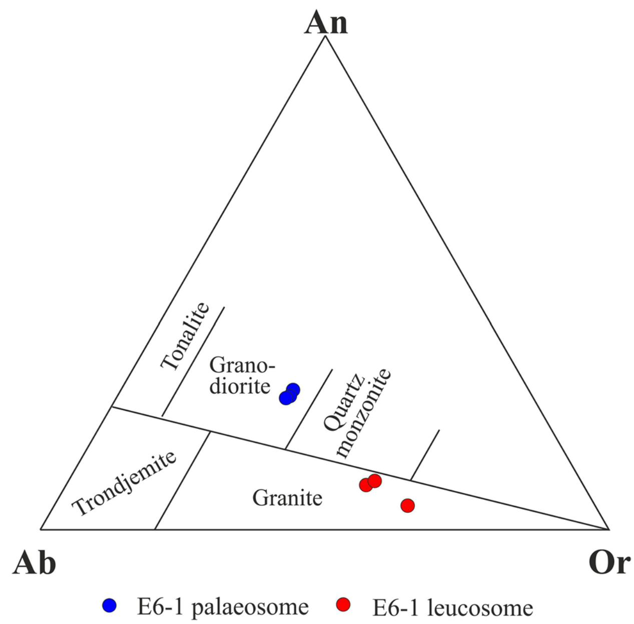

Fig. 4 Normative feldspar classification of palaeosome and leucosome according to O'Connor (1965)

Geochemistry

Rock pieces representing both the E6-1 palaeosome and the leucosome were separated and analyzed for major and trace elements (Table 1; Figs. 4, 5, 6, 7, 8, 9). For comparison, the E6-1 data are plotted altogether with major and trace element data for the I-type TIB 0 Askersund granites from the Bergslagen lithotectonic unit in central Sweden (Persson and Wikström 1993; publicly available database of the Geological Survey of Sweden, SGU database) and granodiorites intruded during the Pilsotas phase of the Kuršiai batholith in western Lithuania (Motuza et al. 2008), the A-type late Svecofennian Fellingsbro and Vallentuna granites from the Bergslagen lithotectonic unit in central Sweden (Öhlander and Zuber 1988; SGU database) and the S-type late Svecofennian Nuuksio granites from the LSGM zone in southern Finland (Nironen and Kurhila 2008).

In the normative feldspar classification diagram after O'Connor (1965), palaeosome has granodioritic composition and the leucosome is compositionally granitic (Fig. 4). The palaeosome tends to have higher contents of FeOt, MgO, Na_2O, TiO_2 and P_2O_5 than the leucosome. This pattern is interrupted in the K_2O vs. SiO_2 diagram (Fig. 5c) by a much higher K_2O content (~ 7 wt%) in the leucosome compared to the palaeosome (~ 3.5 wt%). Selected trace element variations are plotted in the SiO_2 variation diagrams in Fig. 6 and in the primitive mantle-normalized plots in Fig. 7. The leucosome is enriched in incompatible large ion lithophile elements (LILE) Sr (209 ppm), Rb (224 ppm), Ba (876 ppm) and depleted in high field strength elements

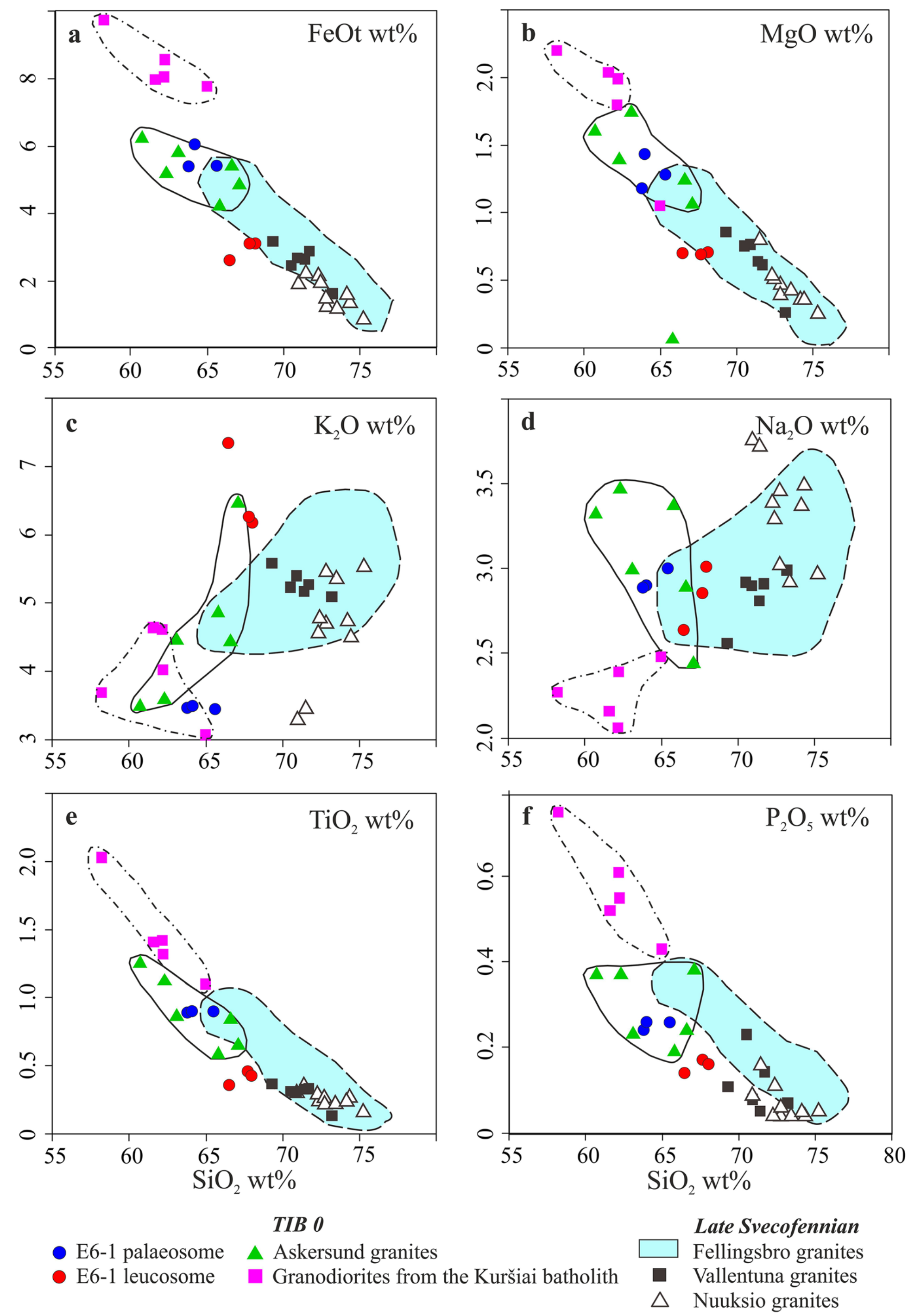

Fig. 5 Harker diagrams showing the major element composition of the E6-1 migmatitic orthogneiss (palaeosome and leucosome) compared with the TIB 0 Askersund granites (Persson and Wikström 1993; SGU database), granodiorites of the Kuršiai batholith (Motuza et al. 2008), late Svecofennian Fellingsbro and Vallentuna granites from the Bergslagen lithotectonic unit (Öhlander and Zuber 1988; SGU database) and late Svecofennian Nuuksio granites from the LSGM zone in southern Finland (Nironen and Kurhila 2008). **a** FeOt vs. SiO$_2$; **b** MgO vs. SiO$_2$; **c** K$_2$O vs. SiO$_2$; **d** Na$_2$O vs. SiO$_2$; **e** TiO$_2$ vs. SiO$_2$; **f** P$_2$O$_5$ vs. SiO$_2$. Blue circle—E6-1 palaeosome; red circle—E6-1 leucosome; green triangles—TIB 0 granites; pink squares—granodiorites from the Kuršiai batholith; grey squares—Vallentuna granites; empty triangles—Nuuksio granites; blue shaded area—Fellingsbro granites

(HFSE) e.g. Zr (105 ppm) and P. Although Nb belongs to the HFSE, its content in the leucosome is extremely high (39 ppm) compared to that in the palaeosome (9 ppm). Ta bears similar chemical characteristics to Nb, but Ta abundance both in the leucosome and palaeosome is similar (0.7 and 0.6 ppm accordingly).

Both palaeosome and leucosome have volcanic-arc granite features in the tectonic discrimination diagram by Pearce et al. (1984; Fig. 8). The REE patterns are shown in Fig. 8. Both the palaeosome and leucosome are characterized by comparatively low REE content and display two different REE patterns. The palaeosome has a fractionated REE pattern with LREE enrichment, low HREE content and a negative Eu anomaly. In contrast, the leucosome has lower Sm and HREE contents and shows slightly positive or lack of Eu anomaly.

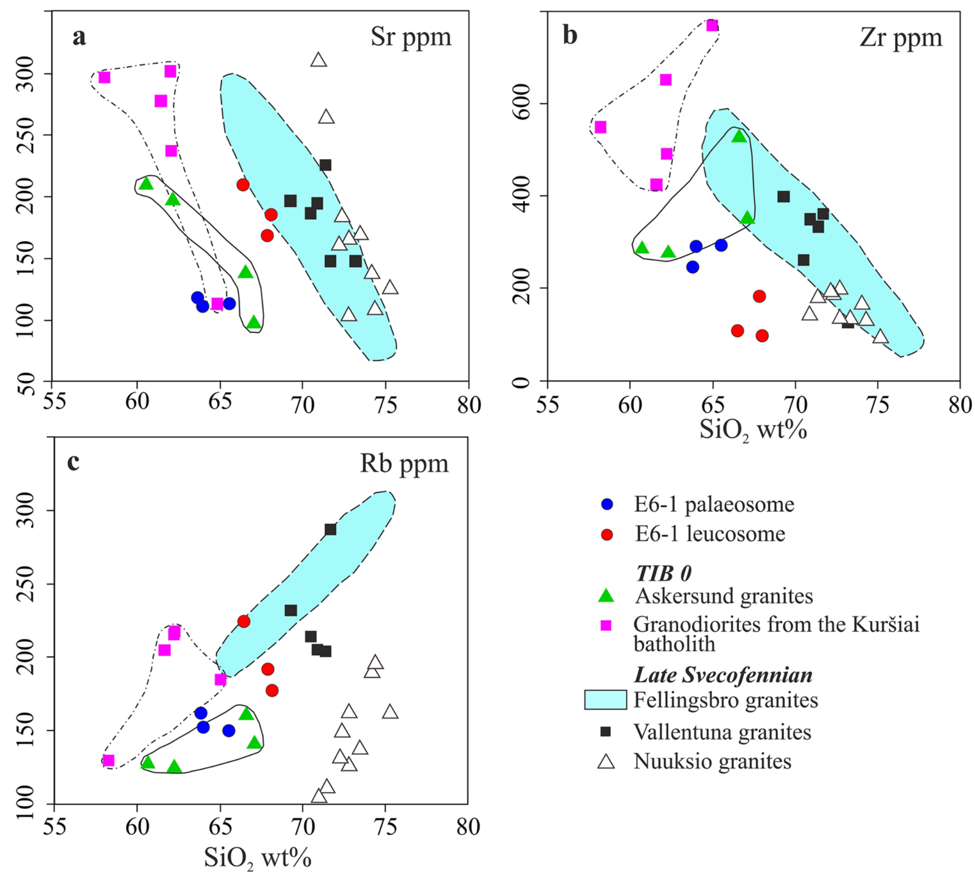

Fig. 6 Harker diagrams showing selected trace element abundances of the E6-1 migmatitic orthogneiss (palaeosome and leucosome). **a** Sr vs. SiO_2; **b** Zr vs. SiO_2; **c** Rb vs. SiO_2. Data sources are as for Fig. 5

U–Pb zircon geochronology

Zircon crystals range ~ 100–200 µm in length and are pink to dark red in color. They are stubby to short-prismatic (length to width ratios < 1.5) and rounded. In BSE images (Fig. 10), zircons are largely homogeneous with faint nebulous or minor sector zoning in some grains. Such textures are common to recrystallized metamorphic zircons, particularly those formed under high-grade conditions and coexisting with anatectic melts (Pidgeon 1992; Pidgeon et al. 1998; Hoskin and Black 2000; Rubatto et al. 2001; Möller et al. 2007). Some zircon grains have dark inherited cores which are surrounded by alteration or inclusions. Oscillatory zoning is not observed in cores or in the recrystallized domains. All grains are fractured, with greater fracture density in the inherited cores (Fig. 10). Inclusions (garnet, apatite and K-feldspar) are rare and mostly appear within or immediately surrounding cores. Although zircons were separated from a composite sample containing both palaeosome and leucosome, the only evidence of separate zircon generations observed are the inherited cores in some grains.

Twenty-three zircon spots from 16 zircon crystals were analyzed (Table 2). Post-analysis inspection of the analytical spots showed that five of these points are on cracks. As it is impossible to quantify potential contamination within cracks, these points have all been excluded from calculations, even if they do not present as outliers. Two spots from inherited zircon cores have low Pb (47 and 54 ppm) and low U (113 and 130 ppm) contents, as well as Th/U ratios of 0.45 and 0.47 (Fig. 11a). Their $^{207}Pb/^{206}Pb$ apparent ages are 1859 and 1844 Ma, respectively. All analysed spots are ~100% concordant, as can be seen in the Table 2. The remaining data show a wide spread in $^{207}Pb/^{206}Pb$ apparent ages spanning from ca. 1845 to ca. 1801 Ma (Fig. 11b). These zircons are characterized by higher Pb (224–606 ppm) and higher U (580–1556 ppm) contents as well as lower Th/U ratios ranging from 0.08 to 0.19. Metamorphic zircon, including that in equilibrium with anatectic melt, characteristically has distinctly lower Th/U ratios than that of magmatic zircon (e.g. Rubatto et al. 2001; Hoskin and Schaltegger 2003).

Discussion

Geochemical correlation

The southern part of the Svecofennian Domain has been intruded by various felsic rocks (I-, A- and S-type granites), which have different origin and different chemical composition. When looking for a possible protolith correlation, the

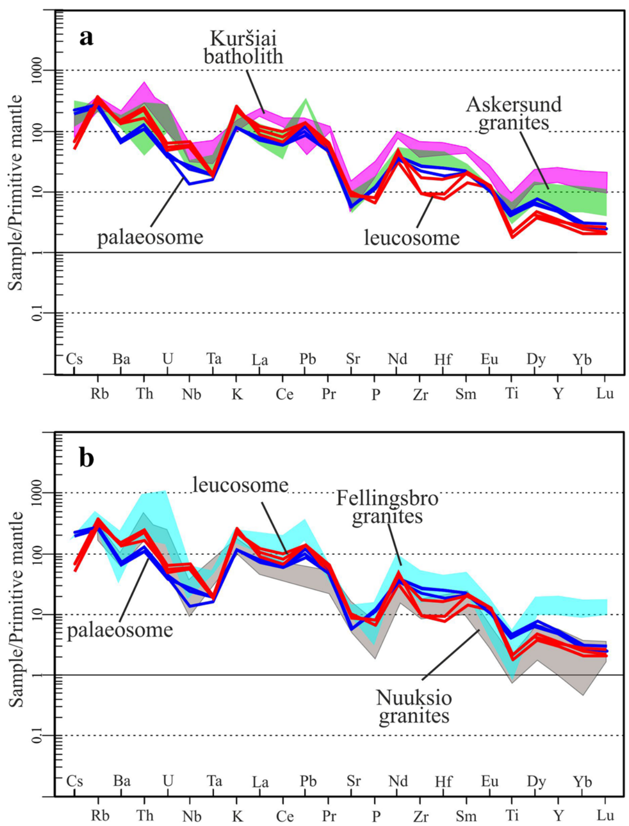

Fig. 7 Primitive mantle-normalized trace element abundances. **a** E6-1 palaeosome and leucosome compared with the TIB 0 Askersund granites and granodiorites of the Kuršiai batholith; **b** E6-1 palaeosome and leucosome compared with the late Svecofennian Fellingsbro granites from the Bergslagen lithotectonic unit and late Svecofennian Nuuksio granites from the LSGM zone in southern Finland. Blue line—E6-1 palaeosome; red line—E6-1 leucosome; green area—TIB 0 granites; pink area—granodiorites from the Kuršiai batholith; blue area—Fellingsbro granites; grey area—Nuuksio granites. Both diagrams after McDonough and Sun (1995)

E6-1 migmatite was compared with the I-type TIB 0 Askersund granites and granodiorites of the Kuršiai batholith and the S-type late Svecofennian granites (Nuuksio granites) from the LSGM zone in southern Finland. In general, the late Svecofennian magmatism in the Bergslagen lithotectonic unit is younger than within the LSGM zone, but the 1.80 Ga A-type late Svecofennian Fellingsbro and Vallentuna granites were also chosen for comparison.

Variation diagrams (Fig. 5), demonstrate good correlation between the E6-1 palaeosome and the Askersund granite fields, expressed in a decrease of FeOt, MgO, Na_2O, TiO_2 and P_2O_5 with increasing SiO_2 contents. The Kuršiai granodiorites have similar trends in the above-mentioned diagrams, but shift towards higher contents of FeOt (8–10 wt%), MgO (1.7–2.3 wt%) and P_2O_5 (0.4–0.8 wt%); the Na_2O content in the Kuršiai granodiorite is also lower (2.0–2.5 wt%). All late Svecofennian granites scatter with more felsic compositions compared to the E6-1 palaeosome. Other major element compositions (except K_2O) are similar to the Fellingsbro granite; however, FeOt, MgO, TiO_2 contents in the Vallentuna and Nuuksio granites are much lower than in the E6-1 palaeosome. The late Svecofennian Fellingsbro granites have a large scatter in Fig. 5, which overlaps the field of the Askersund granites. In spite of this overlap, the palaeosome composition plots always close to the Askersund granites.

Harker diagrams for trace elements (Fig. 6) demonstrate similarities between the E6-1 palaeosome and the Askersund granites, as well as in some cases (Sr, Rb) with the Kuršiai granodiorites. There is also considerable overlap between the palaeosome and the Askersund granites in the multi-element plot (Fig. 7a). By contrast, the Fellingsbro and Nuuksio granites have much higher contents of Ba, Th, U, Ta and Nb, whereas the Nuuksio granites have stronger troughs for P, Zr and Ti (Fig. 7b).

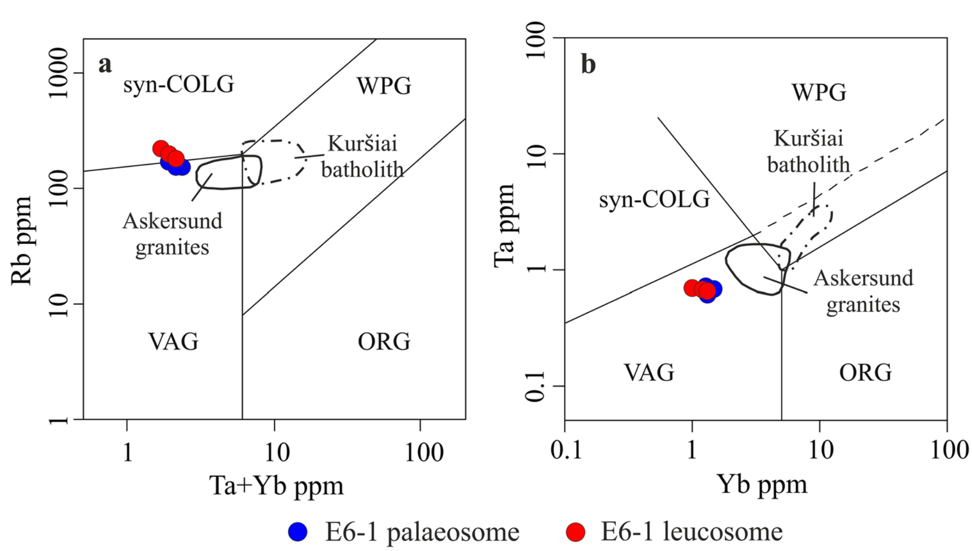

Fig. 8 Selected tectonic discrimination diagrams for the E6-1 migmatitic orthogneiss (palaeosome and leucosome). **a** Rb vs. Ta + Yb diagram, **b** Ta vs. Yb diagram. Blue circle—E6-1 palaeosome; red circle—E6-1 leucosome; solid line—TIB 0 granites, dashed line—granodiorites from the Kuršiai batholith. Both diagrams after Pearce et al. (1984)

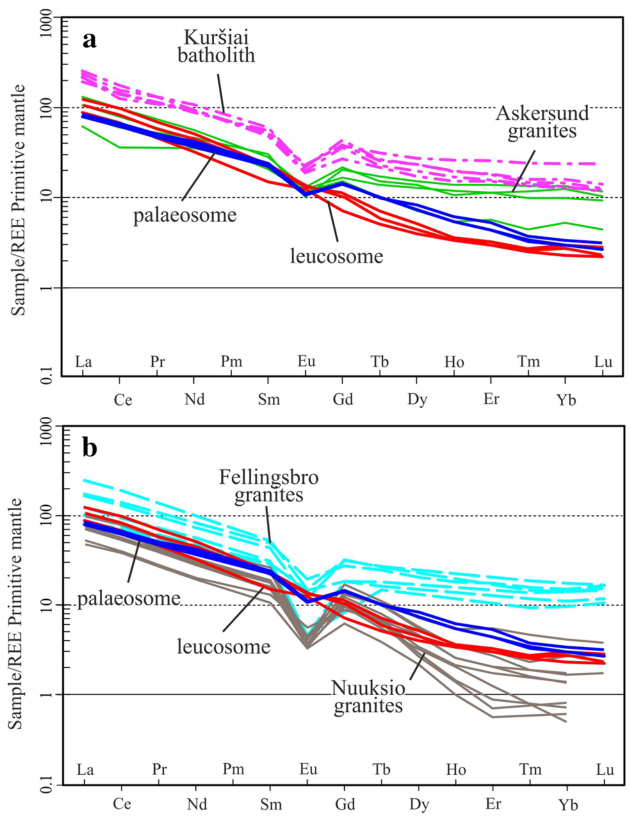

Fig. 9 Primitive mantle-normalized REE abundances. **a** E6-1 palaeosome and leucosome compared with the TIB 0 Askersund granites and granodiorites of the Kuršiai batholith; **b** E6-1 palaeosome and leucosome compared with the late Svecofennian Fellingsbro granites from the Bergslagen lithotectonic unit and late Svecofennian Nuuksio granites from the LSGM zone in southern Finland. Blue line—E6-1 palaeosome; red line—E6-1 leucosome; solid green line—TIB 0 granites; pink dashed line—granodioties from the Kuršiai batholith; blue dashed line—Fellingsbro granites; solid grey line—Nuuksio granites. Both diagrams after McDonough and Sun (1995). Data sources are as for Fig. 5

In spite of a shift towards higher REE abundances, the Kuršiai granodiorites and the Askersund granites have similar patterns with negative slopes and small negative Eu anomalies (Fig. 9a). REEs in the palaeosome plot mostly within the lower part of the TIB 0 field, however, the E6-1 palaeosome is depleted in HREE (Er, Tm, Yb and Lu) relative to TIB 0. Besides a higher variability in the Eu abundances, the REE pattern for the Fellingsbro granites is also similar to the Kuršiai granodiorites (Fig. 9b). The E6-1 palaeosome does not correlate with the Nuuksio granites, which have a pronounced negative Eu anomaly. Previous correlations have been made between TIB 0 and the Kuršiai granodiorites (e.g. Motuza and Motuza 2011); the data presented here support this conclusion. The E6-1 palaeosome shows greater similarity to the Askersund (TIB 0) granites, but in general is more fractionated and with lower HREE than in these granites, indicating a different source or different PT conditions of melting.

In the discrimination diagrams after Pearce et al. (1984), the Askersund granites plot transitionally between the fields for the volcanic-arc granites (VAG) and within-plate granites, but dominantly within the VAG field (Fig. 8). The same characteristics are observed for the E6-1 palaeosome, albeit with the lower HREE. In turn, the Kuršiai granodiorites and the late Svecofennian Fellingsbro granites systematically have an A-type affinity shown by higher Ga/Al ratios (not plotted). This conforms with the within-plate granite signatures seen for the Kuršiai granodiorites in Fig. 8.

In the variation diagrams for major and trace elements (Figs. 5, 6), the leucosome granite shows an affinity towards the late Svecofennian granites in Bergslagen and the LSGM zone. The high K_2O content (Fig. 5c) in the E6-1 leucosome can be explained by melting of the K-rich phases (e.g. biotites and K-feldspars).

The leucosome granite plots within the field of the late Svecofennian Fellingsbro granites in the Sr and Rb vs. SiO_2 diagrams (Fig. 6a, c). The Zr content of the former is, however, closer to the late Svecofennian Nuuksio granite with Zr compositions ranging from 50 to 200 ppm (Fig. 6b). Although similar to the Fellingsbro granites, the E6-1 leucosome granite differs by the high Nb content. This can be explained by biotite melting involved in the leucosome formation: decomposing biotite released Ti, which was consumed for rutile crystallization, in turn Nb was partitioned.

Melt formation

Geochemical data for the E6-1 migmatite show that the leucosome is characterized by a more felsic and alkalic composition relative to palaeosome (Fig. 5), as well as higher contents of Rb, Ba, Sr, U and Th, which tend to be enriched in the melt, and lower contents of immobile elements (Zr, Ti, P and HREE; Figs. 6, 7), which stay in the restite. Together with thin section studies, this suggests that the granite was formed due to partial melting of the palaeosome granodiorite. This is also inferred from the $(La/Yb)_{PM}$ ratios (Table 1, Fig. 9). The LREE (La) are more incompatible compared to HREE (Yb), which causes enrichment of the LREE and depletion of HREE in the melt relative to the restite (Rollinson 1993). Thus the rock formed from the melt has higher $(La/Yb)_{PM}$ ratios than the rock formed from the restite. The leucosome granite studied here has higher $(La/Yb)_{PM}$ ratios compared to the palaeosome granodiorite. This, combined with the slight depletion of HREE in the palaeosome relative to TIB 0, strongly supports a model of formation of the granitic leucosomes from a TIB 0 type granodioritic protolith.

The observed mineral assemblage of the palaeosome suggests that the anatectic melt was produced due to fluid-absent biotite dehydration melting as a source of the leucosome

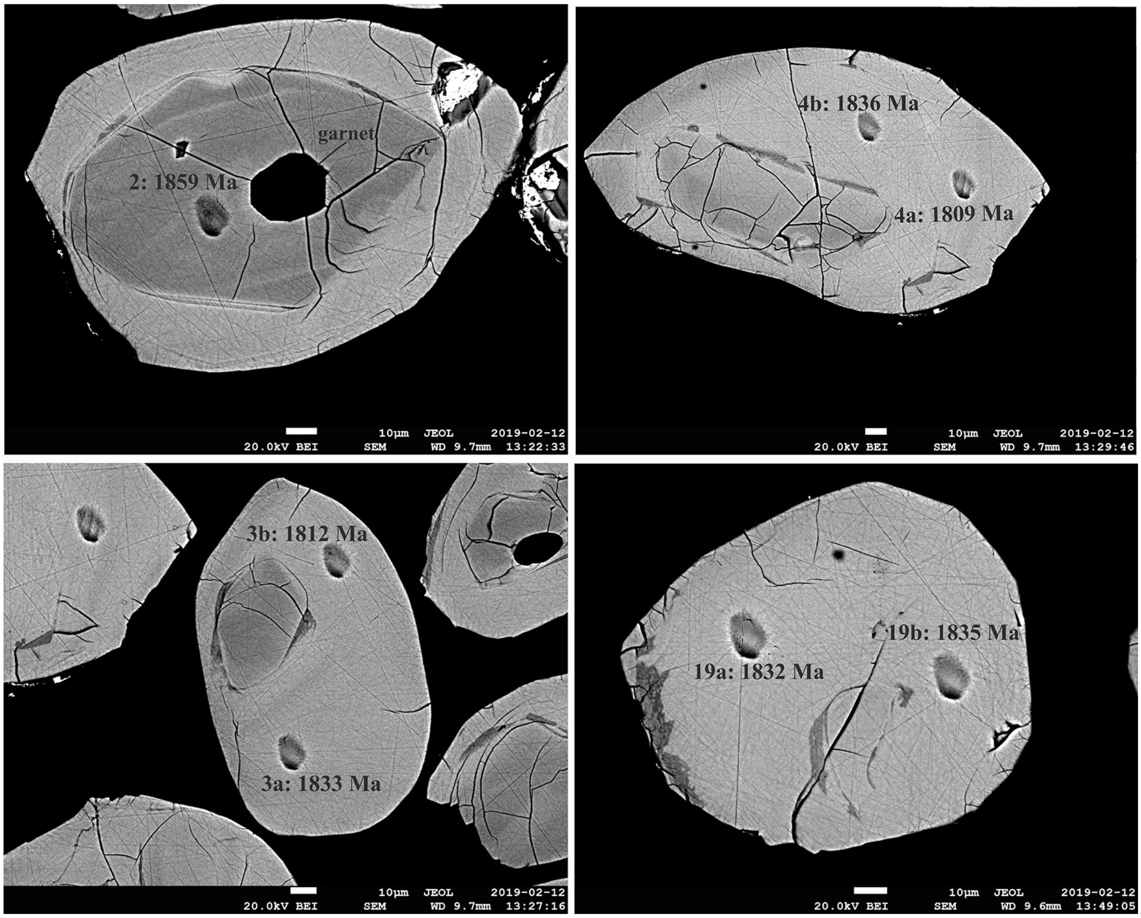

Fig. 10 Selected BSE images of U–Pb dated zircon grains from the E6-1 granodioritic orthogneiss. Spot sites, corresponding analysis numbers and $^{207}Pb/^{206}Pb$ ages are indicated (see Table 2 for individual U–Pb data)

granite (e.g. Patiño Douce and Beard 1995; Patiño Douce and McCarthy 1998). Although leucosome compositions usually do not match a typical melt composition, formation of leucosomes gives evidence for partial melting and the presence of a melt phase at peak metamorphic conditions (e.g. Nehring et al. 2009, 2010).

As the palaeosome represents the parent rock and the leucosome represents melt, but no restite (melanosome) is observed, modelling is challenging. Moreover, the E6-1 migmatite has undergone sericitic alteration, which may have caused significant change in trace element patterns. However, as it was mentioned above, leucosome mineralogy evidences peak metamorphic conditions, thus restite composition can be assumed based on existing biotite dehydration reactions (e.gPatiño Douce and Beard 1995; Sawyer 1998). During experimental fluid-absent melting of a biotite gneiss, the biotite breakdown proceeds according to the following reaction (Patiño Douce and Beard 1995):

$$\begin{aligned} \text{Bt} + \text{Pl} + \text{Qtz} &\rightarrow \text{granitic melt} + \text{OPx} \\ &\quad + \text{Fe oxide (magnetite and ilmenite)}, \end{aligned}$$

which occurs at T~850–930 °C and $P = 3$–15 kbar. Dehydration-melting reaction changes at $P > 10$ kbar leading to crystallization of garnet between 10 and 12.5 kbar. Among other minerals at $P = 12.5$ kbar and $T = 930$ °C, quartz, biotite and rutile occur, however clinopyroxene appears while magnetite disappears. Melting of a synthetic granodioritic biotite gneiss in all experiments described by Patiño Douce and Beard (1995) produced a granitic melt in the normative Ab-Or-An classification, which is consistent with the formation of the E6-1 granitic leucosome from the granodioritic protolith (Fig. 4).

The high Rb, Ba and K contents of the leucosome granite indicate that there was insignificant melt loss, thus melting process was isochemical and equilibrium batch melting equation can be applied (Sawyer 1991).

Table 2 SIMS zircon U–Pb dating results from the E6-1 migmatitic orthogneiss

Sample/	$^{206}Pb_c$[1] (%)	Concentration (ppm)			TW isotopic ratios[3] and errors (%)				Conventional concordia isotopic ratios[3] and errors (%)				Rho.[4]	Conc.[5] (%)	Ages and errors (Ma)						Th/U (meas)
Analysis#		Pb[2]	Th	U	$^{238}U/^{206}Pb$	±1σ	$^{207}Pb/^{206}Pb$	±1σ	$^{207}Pb/^{235}U$	±1σ	$^{206}Pb/^{238}U$	±1σ			$^{207}Pb/^{206}Pb$	±1σ	$^{207}Pb/^{235}U$	±1σ	$^{206}Pb/^{238}U$	±1σ	
Magmatic zircon cores: Th/U > 0.4																					
2	0.03	47	51	113	2.9982	1.1584	0.1137	0.6578	5.2277	1.3321	0.3335	1.1584	0.87	99.8	1859	11.9	1857.1	11.4	1855.5	18.7	0.45
8a	0.01	54	61	130	2.9867	1.1624	0.1127	0.7616	5.2040	1.3897	0.3348	1.1624	0.84	101	1843.9	13.8	1853.3	11.9	1861.7	18.8	0.47
Metamorphic zircons: Th/U < 0.2																					
*1**	*0.57*	*286*	*93*	*798*	*3.1522*	*1.0244*	*0.1073*	*2.7062*	*4.6934*	*2.8936*	*0.3172*	*1.0244*	*0.35*	*101.3*	*1754.1*	*49.5*	*1766.1*	*24.5*	*1776.2*	*15.9*	*0.12*
3a	0.01	311	130	801	2.9845	1.0554	0.1120	0.2623	5.1754	1.0875	0.3351	1.0554	0.97	101.7	1832.5	4.8	1848.6	9.3	1862.9	17.1	0.16
3b	0.01	291	117	758	3.0139	1.0237	0.1108	0.2575	5.0667	1.0556	0.3318	1.0237	0.97	101.9	1811.8	4.7	1830.5	9	1847.1	16.5	0.15
4a	0.01	358	82	952	3.0207	1.0176	0.1106	0.3215	5.0475	1.0671	0.3311	1.0176	0.95	101.9	1809	5.8	1827.3	9.1	1843.5	16.3	0.09
4b	0.01	322	116	829	2.9715	1.0670	0.1122	0.2416	5.2076	1.0940	0.3365	1.0670	0.98	101.9	1835.8	4.4	1853.9	9.4	1870	17.3	0.14
*8b**	*0.07*	*234*	*66*	*630*	*3.0669*	*1.0600*	*0.1102*	*0.2922*	*4.9559*	*1.0996*	*0.3261*	*1.0600*	*0.96*	*100.9*	*1803.3*	*5.3*	*1811.8*	*9.3*	*1819.3*	*16.8*	*0.1*
9a	0.02	268	131	692	3.0104	1.0255	0.1125	0.3373	5.1506	1.0795	0.3322	1.0255	0.95	100.5	1839.5	6.1	1844.5	9.2	1848.9	16.5	0.19
9b	0.01	290	115	739	2.9516	1.0550	0.1124	0.2690	5.2496	1.0888	0.3388	1.0550	0.97	102.3	1838.2	4.9	1860.7	9.3	1880.9	17.2	0.16
10	0.01	315	125	833	3.0556	1.0368	0.1115	0.2417	5.0306	1.0646	0.3273	1.0368	0.97	100.1	1823.8	4.4	1824.5	9.1	1825.1	16.5	0.15
17a	0.02	315	78	828	2.9941	1.0436	0.1101	0.2384	5.0712	1.0705	0.3340	1.0436	0.97	103.1	1801.4	4.3	1831.3	9.1	1857.7	16.9	0.09
*17b**	*0.29*	*148*	*55*	*425*	*3.2954*	*1.0495*	*0.1096*	*0.3811*	*4.5842*	*1.1166*	*0.3035*	*1.0495*	*0.94*	*95.3*	*1792.2*	*6.9*	*1746.4*	*9.3*	*1708.4*	*15.8*	*0.13*
18	0.02	224	104	580	3.0119	1.0362	0.1128	0.2782	5.1644	1.0729	0.3320	1.0362	0.97	100.2	1845.2	5	1846.8	9.2	1848.1	16.7	0.18
19a	0.01	606	213	1556	2.9576	1.0372	0.1120	0.2169	5.2202	1.0596	0.3381	1.0372	0.98	102.5	1831.8	3.9	1855.9	9.1	1877.6	16.9	0.14
19b	0.01	414	161	1054	2.9423	1.0326	0.1122	0.2289	5.2565	1.0576	0.3399	1.0326	0.98	102.8	1834.9	4.1	1861.8	9.1	1886	16.9	0.15
*20**	*0.03*	*308*	*113*	*809*	*3.0177*	*1.0520*	*0.1112*	*0.2744*	*5.0797*	*1.0872*	*0.3314*	*1.0520*	*0.97*	*101.4*	*1818.7*	*5*	*1832.7*	*9.3*	*1845.1*	*16.9*	*0.14*
21	0.01	360	131	930	2.9708	1.1261	0.1119	0.2252	5.1947	1.1484	0.3366	1.1261	0.98	102.2	1830.9	4.1	1851.7	9.8	1870.3	18.3	0.14
22	0.01	259	98	668	2.9729	1.0134	0.1125	0.2887	5.2159	1.0537	0.3364	1.0134	0.96	101.6	1839.6	5.2	1855.2	9	1869.2	16.5	0.15
23	0.01	291	70	785	3.0665	1.0326	0.1103	0.2597	4.9602	1.0648	0.3261	1.0326	0.97	100.8	1804.6	4.7	1812.6	9	1819.5	16.4	0.09
24	0.02	244	55	661	3.0773	1.0480	0.1109	0.2641	4.9674	1.0807	0.3250	1.0480	0.97	100	1813.6	4.8	1813.8	9.2	1813.9	16.6	0.08
*25a**	*0.03*	*323*	*135*	*840*	*3.0107*	*1.0589*	*0.1096*	*0.2825*	*5.0188*	*1.0959*	*0.3321*	*1.0589*	*0.97*	*103.1*	*1792.6*	*5.1*	*1822.5*	*9.3*	*1848.8*	*17*	*0.16*
25b	0.25	317	129	820	2.9955	1.0361	0.1122	0.2653	5.1642	1.0696	0.3338	1.0361	0.97	101.2	1835.2	4.8	1846.7	9.1	1857	16.7	0.16

1. ^{206}Pbc (%)—percentage of common ^{206}Pb in measured ^{206}Pb calculated from the ^{206}Pb calculated from the ^{204}Pb signal (if distinct from background) using age-related common lead after model by Stacey and Kramers (1975)

2. Pb-Th-U concentrations are calculated using standard zircon 91,500

3. Tera-Wasserburg and conventional concordia isotopic ratios corrected for fractionation, blank and age-related common lead (Stacey and Kramers 1975)

4. Rho. is the error correlation between Pb/U errors

5. % concordance = (age($^{206}Pb/^{238}U$)/age($^{207}Pb/^{206}Pb$))*100

*Spot excluded from age calculations. Data from this spot is marked in italic

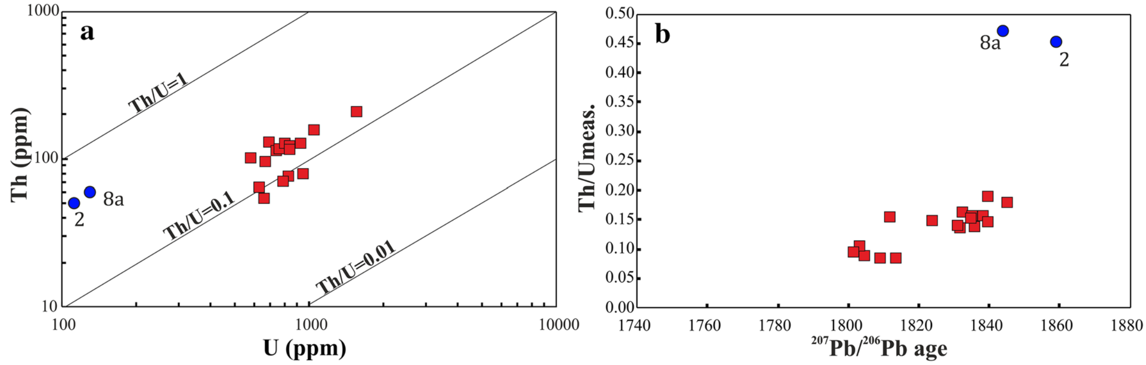

Fig. 11 Th-U systematics in the zircons from the E6-1 migmatitic orthogneiss. **a** Th vs. U concentrations for all analyzed zircons; **b** $Th/U_{meas.}$ vs. $^{207}Pb/^{206}Pb$ ages. Blue circles—magmatic zircon cores (Th/U > 0.4); red squares—metamorphic zircon domains (Th/U < 0.2). Data points not used into calculations are not shown

Concentration of a trace element in the melt (C_L) can be calculated from $C_L = C_O/[d_{RS} + F(1 - d_{RS})]$, where C_O is a trace element concentration in the source rock, d_{RS} is the bulk partition coefficient of the same element in the residual solid, and F is a degree of partial melting. Mineral-melt partition coefficients (D) are presented in Table 3.

The observed mineral assemblage with coexisting rutile and garnet in the leucosome indicates relatively high-pressure and high-temperature melting, which can be modelled using the palaeosome granodiorite as the protolith composition. A theoretical restite consisting of 32% plagioclase, 33% quartz, 6% orthopyroxene, 16% biotite, 5% garnet, 3% titanite, 2% K-feldspar and 1% Fe-Ti oxides (ilmenite, magnetite, and rutile) was used based on fitting the palaeosome mineralogy to the experimental results from Patiño Douce and Beard (1995). Concentrations of P and Zr in the model were controlled by adding trace amounts (less than 1%) of apatite and zircon, respectively. In a model producing 40% melt (Fig. 12), the trace element patterns are close to the observed leucosome composition, although certain elements still show significant deviation as is discussed below.

The modelled melt compositions are distinctly lower in K_2O than the leucosome, which is to be expected because of the evidence of subsequent K metasomatism in the E6-1 samples. The modelled melt composition also has significantly lower Ba and Sr than the observed leucosome composition. If the K metasomatism is related to the intrusion of the nearby lamprophyre dyke, it would be reasonable to assume the same process could be responsible for the elevated Ba and Sr concentrations observed. The inverse is true with Cs, where modelled concentrations are considerably higher than those observed in the leucosome. This can be explained by retention of Cs in the restite due to the strong adsorption potential of biotite, which at these low molar concentrations would be more significant than partitioning (e.g. Lehto et al. 2019). The elevated Nb concentrations and Nb/Ta ratios observed in the leucosome could be produced by kinetic rather than equilibrium fractionation. For example, the diffusion rate of Nb in rutile is much greater than that of Ta (Dohmen et al. 2019), therefore rutile in the restite could have lost disproportionately greater amounts of Nb to the melt, increasing both Nb and Nb/Ta.

Deformation

Thin sections observation suggests that the rock was subject to subsolidus deformation which was sufficient to completely re-crystallize and re-align the quartz (mosaic texture, appearance of triple boundaries, no undulatory extinction) in the leucosome. At microscale, ductile deformation is also evidenced by the dynamic recrystallization of feldspars (perthitic textures in K-feldspars and myrmekitic textures in plagioclases), as well as deformed plagioclase and kinked biotite grains in palaeosomes and leucosomes.

A later deformation event accompanied by K-metasomatism resulted in the calcite + quartz veins and fractures filled with adularia and hematite; this is a common feature within deformation zones (e.g. Barton and Sidle 1994; Ukar and Cloos 2019). These deformation features could be a distal effect from some undetermined adjacent shear zone. The connection between this deformation and the intrusion of the nearby lamprophyre dyke is presently unclear.

Geochronology

A concordia age of 1854 ± 15 Ma was calculated from the two magmatic cores (2σ; Fig. 13). While this determination from limited data is not on its own particularly robust, it coincides with the widespread variably deformed and metamorphosed TIB 0 intrusive rocks in southeastern Sweden (e.g. Åberg and Wikström 1983; Wikström 1991; Persson and Wikström 1993; Andersson et al. 2006), southern

Table 3 Mineral-melt partition coefficients in granodiorites

D	Cs	Rb	Ba	Th	U	Nb	Ta	K	La	Ce	Pb	Pr	Sr	P	Nd	Zr	Hf	Sm	Eu	Ti	Dy	Y	Yb	Lu
Ilmen	0.025	0.025	0.018	0.09	0.09	3	2.7	0.034	0.015	0.012	0.0078	0.011	0.0022	0.002	0.01	2.3	2.4	0.009	0.01	12.5	0.37	0.037	0.13	0.19
Q*	0.029	0.041	0.022	0.009	0.025	0.008	0.008	0.013	0.015	0.015	0.022	0.015	0.022		0.016	0.03	0.03	0.014	0.056	0.038	0.015	0.015	0.017	0.014
Bi	0.63	2.25	6	0.01	0.1	0.085	0.107	3	0.02	0.03	0.1	0.008	0.1	0.005	0.03	0.023	0.023	0.04	0.031	3.5	0.06	0.07	0.11	0.12
Pl	0.087	0.068	1.016	0.095	0.091	0.239	0.053	0.252	0.358	0.339	0.77	0.316	6.65	0.079	0.289	0.078	0.069	0.237	2.17	0.078	0.15	0.138	0.094	0.085
Kf*	4.2	2.85	3.77	0.3	0.017	0.27	0.49	1.39	1.01	0.86	1.46	0.87	2.3		0.51	0.003	0.009	0.42	2.32		0.77	0.017	0.028	0.96
Ap	0.05	0.1	0.45	23	25	0.05	0.05	0.2	12	15	0.1	17	1.4	410	19	16	16	20	13	14	18	162	13	10
Opx	0.047	0.047	0.047	0.13	0.089	0.01	0.126	0.047	0.0003	0.0007	0.047	0.0014	0.047	0.05	0.0028	0.031	0.246	0.0085	0.68	0.5	0.043	0.054	0.125	0.149
Gt	0.0001	0.0007	0.0004	0.0075	0.024	0.04	0.08	0.0013	0.028	0.08	0.032	0.15	0.019	0.184	0.222	0.537	0.431	1.43	1.54	2.63	11.5	14.1	23.2	24.1
Cpx	0.0026	0.01	0.006	0.104	0.032	0.007	0.028	0.0039	0.028	0.059	0.022	0.116	0.032	0.162	0.115	0.125	0.208	0.259	0.341	0.473	0.57	0.603	0.635	0.617
Zrc**				6.1	15	1.6	2.9		0.8	1.7		2.1		2.5	1.5	535	492	2	1.5		5.6	7.8	15	18
Rt	0.01	0.0076	0.0043	0.542	0.2	42.8	68	0.005	0.0057	0.0065	0.0154	0.0073	0.036	0.03	0.0082	3.7	4.97	0.0954	0.00037	45	0.0116	0.0118	0.0126	0.0127
Mgnt	0.001	0.001	0.001	0.02	0.02	0.04	0.04	0.001	0.015	0.016	0.022	0.018	0.022	0.024	0.026	0.12	0.97	0.024	0.025	5	0.018	0.018	0.018	0.018
Tit	0.3	0.5	1.5	0.16	0.14	2.2	6.55	0.7	4.73	7.57	0.04	9	2.68	0.057	12.4	14	2.43	14	13.8	67	8.27	5.42	3.02	2

Ap apatite, *Bi* biotite, *Cpx* clinopyroxene, *Gt* garnet, *Ilmen* ilmenite, *Kf* K-feldspar, *Mgnt* magnetite, *Opx* orthopyroxene, *Pl* plagioclase, *Q* quartz, *Rt* rutile, *Tit* titanite, *Zrc* zircon

*Values for quartz and K-feldspar are compiled from http://earthref.org/KDD/; **Values for zircons are from Rubatto and Hermann (2007) except Nb, Ta, La, Ce and Pr from Nardi et al. (2013); all other values are from Bédard (2006).

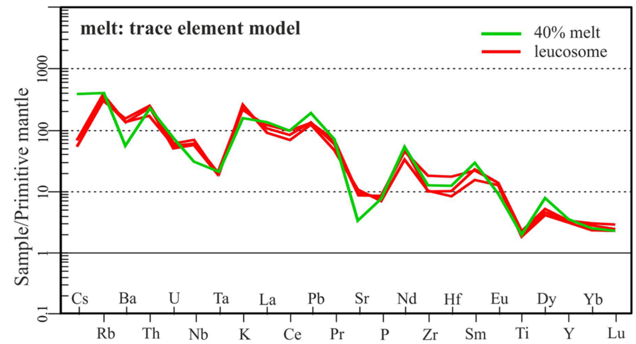

Fig. 12 Modelled trace element composition for formation of the leucosome from 40% partial melting of the palaeosome granodiorite

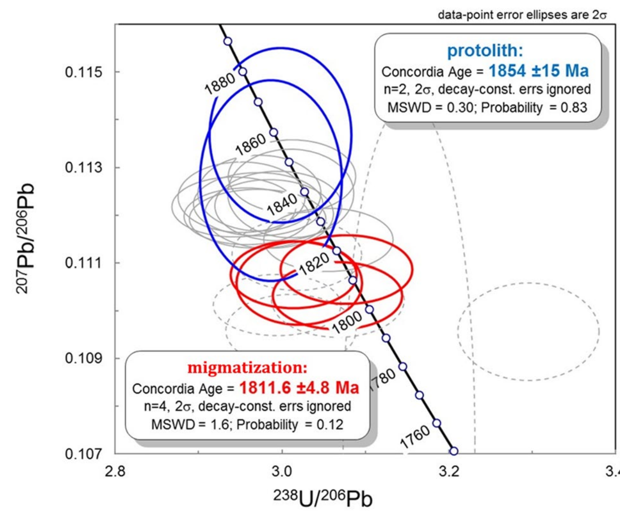

Fig. 13 U–Pb inverse concordia (Tera-Wasserburg) diagram for the inherited magmatic cores (blue ellipses; Th/U > 0.4) and the younger group of metamorphic zircon (red ellipses; Th/U < 0.2). Grey ellipses are not used in the concordia calculations; dashed ellipses are the spots on cracks and are excluded from all calculations. Error ellipses are at the 2σ level. MSWD and probability are calculated for combined concordance and equivalence

Gotland (Salin et al. 2019) and NW Lithuania (Motuza et al. 2008). As such this, combined with the geochemical correlation presented in the previous section, indicates that this represents the igneous protolith age.

The remaining data spread downward along or close to the concordia curve from the concordant magmatic cores. These data are concordant at low end of $^{207}Pb/^{206}Pb$ ratio range but show increasing reverse discordance (older U/Pb ages than $^{207}Pb/^{206}Pb$ ages) with increasing apparent age. The large scatter in the data along concordia can be explained by incomplete resetting of U–Pb compositions due to varying degrees of partial recrystallization of zircons in both palaeosomes and leucosomes. According to Hoskin and Black (2000), the youngest age represents more complete recrystallization, and gives the best estimate for a recrystallization-inducing event. From the four youngest and concordant points, a concordia age of 1812 ± 5 Ma was calculated (2σ, MSWD = 1.6; Fig. 11), which is interpreted as the age of the migmatization. This age correlates with the age of the metamorphic event M2 recorded in the Bergslagen lithotectonic unit of the Svecofennian Domain.

The decreased Th/U ratios of metamorphic zircons are commonly explained by the preferential loss of Th^{4+} over U^{4+} during recrystallization (e.g. Hoskin and Black 2000). As the recrystallized zircons have higher U and Pb contents than the inherited cores, such a simple explanation does not apply. During anatexis, the melt would be expected to be enriched in both U and Th relative to the protolith. This, combined with the higher compatibility of U^{4+} over Th^{4+}, would likely result in an increase in concentrations of both, with a corresponding decrease in Th/U during recrystallization, as is observed here. Similar characteristics were also observed by Möller et al. (2007) in zircons from migmatites from southwestern Sweden.

Reverse discordance is often produced artificially by differential sputtering during SIMS analysis, where it may be easily identified as a horizontal vector in Tera-Wasserburg concordia diagrams (Wiedenbeck 1995; Romer 2003). If the reverse discordance observed here is such an analytical artifact, these horizontal vectors may be disguised by the variation in $^{207}Pb/^{206}Pb$ that result from partial resetting of recrystallized zircons. Other studies have indicated that such discordance only becomes statistically significant in zircons with high U concentrations (> 2500 ppm; Williams and Hergt 2000; White and Ireland 2012), which is not the case here.

Alternatively, reverse discordance can be the result of a natural process involving gain of radiogenic Pb or removal of U (e.g. McFarlane et al. 2005; Corfu 2013; Kusiak et al. 2013). In such cases, data tend to form a linear discordia array similar to that observed in regular discordant data, in which intercepts indicate the timing of the crystallization (upper) and of disturbance (lower) events (e.g. McFarlane et al. 2005). The upper intercept of this discordia is at 1814 ± 40 Ma (95% confidence; MSWD = 1.02; Fig. 14), or very similar to the calculated concordia despite the much larger uncertainty in age. Using this unconstrained regression, the lower intercept is at 1016 ± 860 Ma. By assuming that the concordia age reflects the crystallization of these zircon domains, a discordia may be anchored to 1812 ± 5 Ma, in which case a lower intercept of 1066 ± 5 Ma is produced. This result likely grossly underestimates the error in this age population; therefore, a Monte Carlo solution was calculated giving a lower intercept of 1073 + 230/ − 210 Ma (95% confidence; MSWD = 0.92). While this is a very large range of uncertainty, these results consistently indicate that

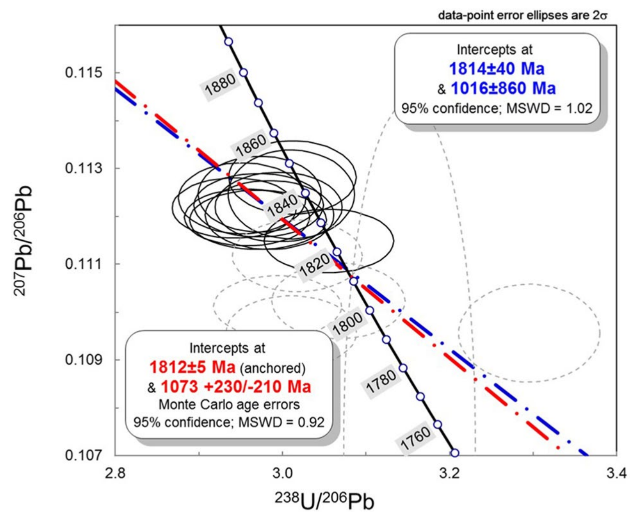

Fig. 14 U–Pb inverse concordia (Tera-Wasserburg) diagram for the reverse discordant zircon population. Grey dashed ellipses are the spots on cracks and are excluded from calculations. Error ellipses are at the 2σ level. See text for discussion

disturbance occurred during the early part of the Sveconorwegian orogeny at 1.1–1.0 Ga (Bingen et al. 2005).

As a consequence of recognizing that the geochemical pattern and the age of the protolith in the E6-1 drill core is comparable with the TIB 0 granitoids, the host rock into which this protolith intruded must have been older than 1854 Ma. Since there are no indications of any rock units older than the Svecofennian in the Baltic Sea region, the only realistic alternative is thus that the host rock to the E6-1 protolith belongs to the Svecofennian Domain. This means that the southwestern border of the Svecofennian Domain must be located between the site for the E6-1 drill hole and the site for the E7-1 drill hole, where a granitoid belonging to the TIB 1b generation has been identified (Salin et al. 2019).

Conclusion

Analyses of major and trace element compositions in the E6-1 migmatitic orthogneiss reveal that the protolith composition correlates with the TIB 0 Askersund granites of the Transscandinavian Igneous Belt in southeastern Sweden. Both E6-1 protolith and the TIB 0 Askersund granites show affinity towards the volcanic-arc setting. The granitic leucosome was formed due to fluid-absent biotite dehydration melting of the granodioritic protolith represented by the palaeosome. It shows geochemical similarities to other late Svecofennian anatectic melts.

Inherited zircon cores from the the E6-1 migmatitic orthogneiss show that the age of the magmatic protolith is 1854 ± 15 Ma. This age fits well with the ages of both variable deformed and metamorphosed TIB 0 granitoids and corroborates the geochemical correlation with the TIB 0 Askersund granites. The leucosome developed via partial melting of the TIB 0 protolith at 1812 ± 5 Ma, which correlates with the M2 metamorphic event in the Bergslagen lithotectonic unit. Reverse discordance may be the result of minor U–Pb disturbance occurring during the early part of the Sveconorwegian orogeny.

Geochemical and geochronological evidence suggests that the E6-1 drill site is located within the Svecofennian Domain. Combined with the evidence from the E7-1 drill site ca. 55 km to the southwest and outside the Svecofennian Domain (Salin et al. 2019), the southwestern border of the Svecofennian Domain must lie between these sites.

Acknowledgements The authors would like to thank the Geological Survey of Latvia for the opportunity to use sample material from the E6-1 drill core. The Geological Survey of Sweden (SGU) is acknowledged for providing geochemical reference data. Marja Lehtonen (Finnish Geoscience Research Laboratory, Espoo, Finland) is acknowledged for the help with the SEM imaging. The staff of the Nordsim laboratory (Stockholm) is acknowledged for the SIMS analytical work: Kerstin Lindén for preparation of a zircon epoxy mount and Martin Whitehouse for data reduction. This is a Nordsim contribution № 670 …. Financial support for the Nordsim laboratory work was provided by the Finnish Society of Sciences and Letters.

Funding Open access funding provided by University of Turku (UTU) including Turku University Central Hospital.

References

Åberg G, Wikström A (1983) Radiometric dating of the postorogenic Graversfors granite, south central Sweden. Geologiska Föreningens i Stockholms Förhandlingar 104:225–230

Åhäll K-I, Connelly JN, Brewer TS (2002) Transitioning from Svecofennian to Transcandinavian Igneous Belt (TIB) magmatism in SE Sweden: implications from the 1.82 Ga Eksjö tonalite. GFF 124:217–224

Ahl M, Andersson UB, Lundqvist T, Sundblad K (1996) Rapakivi granites and related rocks in central Sweden. Sveriges geologiska undersökning Ca 87

Ahl M, Bergman S, Bergström U, Eliasson T, Ripa M, Weihed P (2001) Geochemical classification of plutonic rocks in central and northern Sweden. Sveriges geologiska undersökning, Rapporter och meddelanden, p 106

Allen RL, Lundström I, Ripa M, Christofferson H (1996) Facies analysis of a 1.9 Ga, continental margin, back-arc, felsic caldera province with diverse Zn-Pb-Ag-(Cu-Au) sulfide and Fe oxide deposits, Bergslagen region. Sweden Econ Geol 91:979–1008

Andersson UB (1997) The late Svecofennian, high-grade contact and regional metamorphism in southwestern Bergslagen (central southern Sweden). Sveriges geologiska undersökning, Rapporter och meddelanden, p 970519 (**Final report**)

Andersson UB, Högdahl K, Sjöström H, Bergman S (2006) Multistage growth and reworking of the Palaeoproterozoic crust in the Bergslagen area, southern Sweden: evidence from U-Pb geochronology. Geol Mag 143:679–697

BABEL Working group (1993) Deep seismic reflection/refraction interpretation of crustal structure along BABEL profiles A and B in the southern Baltic Sea. Geophys J Int 112:325–343

Barton M, Sidle WC (1994) Petrological and geochemical evidence for granitoid formation: The Waldoboro pluton complex, Maine. J Petrol 35:1241–1474

Bédard JH (2006) A catalytic delamination-driven model for coupled genesis of Archaean crust and sub-continental lithospheric mantle. Geochim Cosmochim Acta 70:1188–1214

Bergström U, Juhojuntti N, Kero L, Lundqvist L, Stephens M, Sukotjo S, Wik N-G, Wikman H (2002) Projekt Småland, regionalt berg. In: Delin H (ed) Regional berggrundsgeologisk undersökning. Sammanfattning av pågående undersökningar, Uppsala, pp 65–83 (**Geological Survey of Sweden**)

Beunk FF, Page LM (2001) Structural evolution of the accretional continental margin of the Paleoproterozoic Svecofennian orogen in southern Sweden. Tectonophysics 339:67–92

Bingen B, Skår Ø, Marker M, Sigmond EMO, Nordgulen Ø, Ragnhildstveit J, Mansfeld J, Tucker RD, Liégeois J-P (2005) Timing of continental building in the Sveconorwegian orogen, SW Scandinavia. Norwegian J Geol/ Norsk Geologisk Forening 85:87–116

Bogdanova S, Gorbatschev R, Grad M, Janik T, Guterch A, Kozlovskaya E, Motuza G, Skridlaite G, Starostenko V, Taran L, Eurobrodge and Polonaise Working Groups (2006) EUROBRIDGE: new insight into the geodynamic evolution of the East European Craton. In: Gee DG and Stephenson RA (eds) European Lithosphere Dynamics. Geological Society, London, Memoirs 32:599–625

Bogdanova S, Gorbatschev R, Skridlaite G, Soesoo A, Taran L, Kurlovich D (2015) Trans-Baltic Palaeoproterozoic correlations towards the reconstruction of supercontinent Columbia/Nuna. Precambr Res 259:5–33

Claesson S, Bogdanova S, Bibikova EV, Gorbatschev R (2001) Isotopic evidence for Palaeoproterozoic accreation in the basement of the East European Craton. Tectonophysics 339:1–18

Corfu F (2013) A century of U-Pb geochronology: the long quest towards concordance. GSA Bull 125:33–47

Dohmen R, Marschall HR, Ludwig T, Polednia J (2019) Diffusion of Zr, Hf, Nb and Ta in rutile: effects of temperature, oxygen fugacity, and doping level, and relation to rutile point defect chemistry. Phys Chem Miner 46:311–332

EUROBRIDGE seismic working group (1999) Seismic velocity structure across the Fennoscandia-Sarmatia suture of the East European Craton beneath the EUROBRIDGE profile through Lithuania and Belarus. Tectonophysics 314:193–217

Gaál G, Gorbatschev R (1987) An outline of the Precambrian evolution of the Baltic Shield. Precambr Res 35:15–52

GERM Partition Coefficient (Kd) Database. http://earthref.org/KDD/

Grigelis A (ed) (1991) Geology and geomorphology of the Baltic Sea. Lithuanian Geological Institute, Nedra

Hermansson T, Stephens MB, Corfu F, Andersson J, Page L (2007) Penetrative ductile deformation and amphibolite-facies metamorphism prior to 1851 Ma in the western part of the Svecofennian orogen, Fennoscandian Shield. Precamb Res 153:29–45

Hoskin PWO, Black LP (2000) Metamorphic zircon formation by solid-state recrystallization of protolith igneous zircon. J Metamorph Geol 18:423–439

Hoskin PWO, Schaltegger U (2003) The composition of zircon in igneous and metamorphic petrogenesis. Rev Mineral Geochem 53:27–62

Jarl L-G, Johansson Å (1988) U-Pb zircon ages of granitoids from the Småland-Värmland granite-porphyry belt, southern and central Sweden. Geologiska Föreningens i Stockholms Förhandlingar 110:21–28

Johansson Å, Stephens MB (2017) Timing of magmatism and migmatization in the 2.0–1.8 Ga accretionary Svecokarelian orogen, south-central Sweden. Int J Earth Sci 106:783–810

Kampmann TC, Stephens MB, Ripa M, Hellström FA, Majka J (2016) Time constraints on magmatism, mineralisation and metamorphism at the Falun base metal sulphide deposit, Sweden, using U-Pb geochronology on zircon and monazite. Precamb Res 278:52–68

Kirs J, Haapala I, Rämö OT (2004) Anorogenic magmatic rocks in the Estonian crystalline basement. Proceedings of the Estonian Academy of Sciences. Geology 53:210–225

Kleinhanns IC, Whitehouse MJ, Nolte N, Baero W, Wilsky F, Hansen BT, Schoenberg R (2015) Mode and timing of granitoid magmatism in the Västervik area (SE Sweden, Baltic Shield): Sr–Nd isotope and SIMS U-Pb age constraints. Lithos 212–215:321–337

Korja A, Heikkinen P (2005) The accretionary Svecofennian orogeny—insight from the BABEL profiles. Precamb Res 136:241–268

Korja A, Lahtinen R, Nironen M (2006) The Svecofennian orogen: a collage of microcontinents and island arcs. Geol Soc Lond Memoirs 32:561–578

Koistinen T, Stephens MB, Bogatchev V, Nordgulen Ø, Wennerström M, Korhonen J (2001) Geological map of the Fennoscandian shield. Scale 1:2,000,000. Geolog Surv Finl Norw Swed and the North-West Department of Natural Resources of Russia

Kresten P (1972) Der basische Magmatismus und seine Stellung in der geologischen Entwicklung des Västervik-Gebiets, Südostschweden. Geologiska Föreningen i Stockholm Förhandlingar 94:91–109

Kurhila M, Mänttäri I, Vaasjoki M, Rämö OT, Nironen M (2011) U-Pb geochronological constraints of the late Svecofennian leucogranites of southern Finland. Precamb Res 190:1–24

Kusiak MA, Whitehouse MJ, Wilde SA, Nemchin AA, Clark C (2013) Mobilization of radiogenic Pb in zircon revealed by ion imaging: implications for early Earth geochronology. Geology 41:291–294

Larson S-Å, Berglund J (1992) A chronological subdivision of the Transscandinavian Igneous Belt—three magmatic episodes? Geologiska Föreningen i Stockholm Förhandlingar 114:459–461

Lehto J, Puukko E, Lindberg A, Voutilainen M (2019) Batch sorption experiments of cesium and strontium on crushed rock and biotite for the estimation of distribution coefficients on intact crystalline rock. Heliyon 5:e02296

Lindh A (2014) Chemical composition of Late Svecofennian granite in the Bothnian Basin, central Sweden. GFF 136:483–502

Ludwig KR (2003) User's manual for Isoplot 3.00: a geochronlogical toolkit for Microsoft Excel. Berkeley Geochronl Center Special Publication 4:25–32

Lund CE, Gorbatschev R, Smirnov A (2001) A seismic model of the Precambrian crust along the coast of southeastern Sweden: the Coast Profile wide-angle airgun experiment and the southern part of FENNOLORA revisited. Tectonophysics 339:93–111

Mansfeld J (1991) U-Pb age determinations of Småland-Värmland granitoids in Småland, southeastern Sweden. Geologiska Föreningen i Stockholm Förhandlingar 113:113–119

Mansfeld J (1996) Geological, geochemical and geochronological evidence for a new Palaeoproterozoic terrane in southeastern Sweden. Precambr Res 77:91–103

Mansfeld J (2001) Age and ϵ_{Nd} constraints on the Palaeoproterozoic tectonic evolution in the Baltic-Sea region. Tectonophysics 339:135–151

McDonough WF, Sun SS (1995) The composition of the earth. Chem Geol 120:223–253

McFarlane CR, Connelly JN, Carlson WD (2005) Intracrystalline redistribution of Pb in zircon during high-temperature contact metamorphism. Chem Geol 217:1–28

Möller C, Andersson J, Lundqvist I, Hellström F (2007) Linking deformation, migmatite formation and zircon U-Pb geochronology in polymetamorphic orthogneisses, Sveconorwegian Province, Sweden. J Metamorph Geol 25:727–750

Motuza G, Motuza V (2011) Charnockitic rocks in the crystalline basement of Western Lithuania: implications on their origin and correlation with the Askersund suite in SE Sweden. Geol Quart 55:63–70

Motuza G, Motuza V, Salnikova E, Kotov A (2008) Extensive charnockitic-granitic magmatism in the crystalline crust of West Lithuania. Geologija, Vilnius, Petrology 50:1–16

Nardi LVS, Formoso MLL, Müller IF, Fontana E, Jarvis K, Lamarão C (2013) Zircon/rock partition coefficients of REEs, Y, Th, U, Nb, and Ta in granitic rocks: uses for provenance and mineral exploration purposes. Chem Geol 335:1–7

Nehring F, Foley SF, Hölttä P, Van Den Kerkhof AM (2009) Internal differentiation of the Archean continental crust: fluid-controlled partial melting of granulites and TTG–Amphibolite associations in Central Finland. J Petrol 50:3–35

Nehring F, Foley SF, Hölttä P (2010) Trace element partitioning in the granulite facies. Contrib Mineral Petrol 159:493–519

Nironen M, Kurhila M (2008) The Veikkola granite area in southern Finland: emplacement of zia 1.83–1.82 Ga plutonic sequence in an extensional regime. Geol Surv Finl, Bull 80

O'Connor JT (1965) A classification for quartz-rich igneous rocks. Geological Survey Professional Paper 525

Öhlander B, Zuber J (1988) Genesis of the Fellingsbro-type granites: evidence from gravity measurements and geochemistry. Geologiska Föreningen i Stockholm Förhandlingar 110:39–54

Patiño Douce AE, Beard JS (1995) Dehydration-melting of biotite gneiss and quartz amphibolite from 3 to 15 kbar. J Petrol 36:707–738

Patiño Douce AE, McCarthy TC (1998) Melting of crustal rocks during continental collision and subduction. In: Hacker BR, Liou JG (eds) When continents collide: geodynamics and geochemistry of ultrahigh-pressure rocks. Petrol and structural Geol, vol 10. Springer, Dordrecht, pp 27–55

Pearce JA, Harris NB, Tindle AG (1984) Trace element discrimination diagrams for the tectonic interpretation of granitic rocks. J Petrol 25:956–983

Persson P-O, Wikström A (1993) A U-Pb dating of the Askersund granite and its marginal augen gneiss. Geologiska Föreningen i Stockholm Förhandlingar 115:321–329

Pidgeon RT (1992) Recrystallization of oscillatory zoned zircon: some geochronological and petrological implications. Contrib Mineral Petrol 110:463–472

Pidgeon RT, Nemchin AA, Hitchen GJ (1998) Internal structures of zircons from Archaean granites from the Darling Range batholith: implications for zircon stability and the interpretation of zircon U-Pb ages. Contrib Mineral Petrol 132:288–299

Rämö OT, Haapala I (2005) Rapakivi granites. In: Lehtinen M, Nurmi PA, Rämö OT (eds) The Precambrian geology of Finland—key to the evolution of the Fennoscandian Shield. Elsevier Science B.V, Amsterdam, pp 533–562

Rollinson H (1993) Using geochemical data: evaluation, presentation, interpretation. Prentice Hall, Pearson

Romer RL (2003) Alpha-recoil in U-Pb geochronology: effective sample size matters. Contrib Mineral Petrol 145:481–491

Röshoff K (1975) Some aspects of the Precambrian in southeastern Sweden in the light of a detailed geological study of the Lake Nömmen area. Geol Fören Stockholm Förh 97:368–378

Rubatto D, Hermann J (2007) Experimental zircon/melt and zircon/garnet trace element partitioning and implications for the geochronology of crustal rocks. Chem Geol 241:38–61

Rubatto D, Williams IS, Buick IS (2001) Zircon and monazite response to high-grade metamorphism in the Reynolds Range, central Australia. Contrib Mineral Petrol 140:458–468

Salin (2014) Petrology and lead isotopic composition of rocks of the Precambrian basement under Gotland and adjacent off-shore regions of the Baltic Sea. University of Turku, Master's thesis

Salin E, Sundblad K, Woodard J, O'Brien H (2019) The extension of the Transscandinavian Igneous Belt into the Baltic Sea region. Precambr Res 328:287–308

Salin E, Sundblad K, Lahaye Y, Woodard J (2020) Recognition of a 1.85 Ga oceanic rifting environment in southeastern Sweden. EGU General Assembly, abstract volume

Sawyer EW (1991) Disequilibrium melting and the rate of melt–residuum separation during migmatization of mafic rocks from the Grenville Front, Quebec. J Petrol 32:701–738

Sawyer EW (1998) Formation and evolution of granite magmas during crustal reworking: the significance of diatexites. J Petrol 39:1147–1167

Sawyer EW (2008) Atlas of migmatites. The Canadian mineralogist, Special Publication 9. NRC Research Press, Ottawa

Skiöld T (1988) Implications of new U-Pb zircon chronology to early Proterozoic crustal accretion in northern Sweden. Precambr Res 38:147–164

Skridlaite G, Motuza G (2001) Precambrian domains in Lithuania: evidence of terrane tectonics. Tectonophysics 339:113–133

Skridlaite G, Bogdanova S, Taran L, Baginski B (2014) Recurrent high grade metamorphism recording a 300 Ma long Proterozoic crustal evolution in the western part of the East European Craton. Gondwana Res 25:649–667

Skyttä P, Mänttäri I (2008) Structural setting of late Svecofennian granites and pegmatites in Uusimaa Belt, SW Finland: age constraints and implications for crustal evolution. Precambr Res 164:86–109

Stacey JS, Kramers JD (1975) Approximation of terrestrial lead isotope evolution by a two-stage model. Earth Planet Sci Lett 26:207–221

Stephens M (2020) Outboard-migrating accretionary orogeny at 1.9–1.8 Ga (Svecokarelian) along a margin to the continent Fennoscandia. In: Stephens M, Weihed B (eds) Sweden: Lithotectonic framework, tectonic evolution and mineral resources. Geological Society, London, pp 155–206 (**Memoirs 50**)

Stephens M, Weihed B (eds) (2020) Sweden: Lithotectonic framework, tectonic evolution and mineral resources. Geological Society, London (**Memoirs 50**)

Stephens MB, Andersson J (2015) Migmatization related to mafic underplating and intra- or back-arc spreading above a subduction boundary in a 2.0–1.8 Ga accretionary orogen. Sweden Precambr Res 264:235–257

Stephens M, Jansson NF (2020) Palaeoproterozoic (1.9–1.8 Ga) magmatism, sedimentation and mineralization in the Bergslagen lithotectonic unit, Svecokarelian orogen. In: Stephens M, Weihed B (eds) Sweden: Lithotectonic framework, tectonic evolution and mineral resources. Geological Society, London, pp 155–206 (**Memoirs 50**)

Stephens MB, Wahlgren C-H, Weihed P (1997) Sweden. In: Moores EM, Fairbridge RW (eds) Encyclopedia of European and Asian regional geology. Chapman and Hall, London, pp 690–704

Stephens MB, Ripa M, Lundström I, Persson L, Bergman T, Ahl M, Wahlgren C-H, Persson P-O, Wickström L (2009) Synthesis of the bedrock geology in the Bergslagen Region, Fennoscandian Shield, South-Central Sweden. Geological Survey of Sweden Ba 58

Sultan L, Plink-Björklund P (2006) Depositional environments at a Palaeoproterozoic continental margin, Västervik Basin, SE Sweden. Precamb Res 145:243–271

Sultan L, Claesson S, Plink-Björklund P (2005) Proterozoic and Archaean ages of detrital zircon from the Palaeoproterozoic Västervik Basin, SE Sweden: implications for provenance and timing of deposition. GFF 127:17–24

Sundblad K, Mansfeld J, Särkinen M (1997) Palaeoproterozoic rifting and formation of sulphide deposits along the southwestern margin of the Svecofennian Domain, southern Sweden. Precamb Res 82:1–12

Sundblad K, Claesson S, Gyllencreutz R (2003) The Precambrian of Gotland—a key to the understanding of the geologic environment for granitoids in the Baltic Sea region. In: Granitic Systems—State of the Art and Future Avenues, Helsinki, abstract volume, pp 102–106

Ukar E, Cloos M (2019) Cataclastic deformation and metasomatism in the subduction zoneof mafic blocks-in-mélange, San Simeon, California. Lithos 345–346:1–25

Vaasjoki M, Sakko M (1988) The evolution of the Raahe-Ladoga zone in Finland: Isotopic constraints. In: Korsman K (ed.) Tectonometamorphic evolution of the Raahe-Ladoga zone. Geological Survey of Finland, Bulletin 343, pp 7–32

Väisänen M, Mänttäri I, Hölttä P (2002) Svecofennian magmatic and metamorphic evolution in southwestern Finland as revealed by U-Pb zircon SIMS geochronology. Precambr Res 116:111–127

Wahlgren C-H, Stephens M (2020) Småland lithotectonic unit dominated by Paleoproterozoic (1.8 Ga) syn-orogenic magmatism, Svecokarelian orogen. In: Stephens M, Weihed B (eds) Sweden: Lithotectonic framework, tectonic evolution and mineral resources. Geological Society, London, pp 207–235 (**Memoirs 50**)

Welin E (1992) Isotopic results of the Proterozoic crustal evolution of south-central Sweden; review and conclusions. Geologiska Föreningen i Stockholm Förhandlingar 114:299–312

White LT, Ireland TR (2012) High-uranium matrix effect in zircon and its implications for SHRIMP U-Pb age determinations. Chem Geol 306–307:78–91

Whitehouse MJ, Kamber B (2005) Assigning dates to thin gneissic veins in high-grade metamorphic terranes: a cautionary tale from Akilia, southwest Greenland. J Petrol 46:291–318

Whitehouse MJ, Kamber BS, Moorbath S (1999) Age significance of U-Th-Pb zircon data from early Archaean rocks of west Greenland—a reassessment based on combined ion-microprobe and imaging studies. Chem Geol 160:201–224

Wiedenbeck M (1995) An example of reverse discordance during ion microprobe zircon dating: an artifact of enhanced ion yields from a radiogenic labile Pb. Chem Geol 125:197–218

Wiedenbeck M, Hanchar JM, Peck WH, Sylvester P, Valley J, Whitehouse M, Kronz A, Morishita Y, Nasdala L, Fiebig J, Franchi I (2004) Further characterization of the 91500 zircon crystal. Geostand Geoanal Res 28:9–39

Wik N-G, Bergström U, Claeson D, Juhojuntti N, Kero L, Lundqvist L, Petersson J, Sukotjo S, Wedmark M, Wikman H (2003) Regionala kartor 1:250,000. Projekt Småland regional berg. In: Delin H (ed) Berggrundsgeologisk undersökning. Sammanfattning av pågående verksamhet 2002. Geol. Surv. Sweden, Rapporter och meddelanden 112:96–116

Wik N-G, Bergström U, Bruun Å, Claeson D, Jelinek C, Juhojuntti N, Kero L, Lundqvist L, Stephens MB, Sukotjo S, Wikman H

(2005) Beskrivning till regional berggrundskarta över Kalmar län. Geological Survey of Sweden Ba 66

Wikström A (1991) Structural features of some younger granitoids in central Sweden and implications for the tectonic subdivision of granitoids. Precambr Res 51:151–159

Wikström A (1996) U-Pb zircon dating of a coarse porphyritic quartz monzonite and even grained, grey tonalitic gneiss from Tiveden area, south central Sweden. Geol Survey Sweden C 828:41–47

Williams IS, Hergt JM (2000) U-Pb dating of Tasmanian dolerites: a cautionary tale of SHRIMP analysis of high-U zircon. In: Woodhead JD, Hergt JM, Noble WP (eds) Beyond 2000: new Frontiers in isotope geoscience: Victoria. University of Melbourne, Australia, pp 185–188